

## DISCLAIMER

DE83 007963

This report was prepared as an account of work sponsored by an agency of the United States Government. Neither the United States Government nor any agency thereof, nor any of their employees, makes any warranty, express or implied, or assumes any legal liability or responsibility for the accuracy, completeness, or usefulness of any information, apparatus, product, or process disclosed, or represents that its use would not infringe privately owned rights. Reference herein to any specific commercial product, process, or service by trade name, trademark, manufacturer, or otherwise does not necessarily constitute or imply its endorsement, recommendation, or favoring by the United States Government or any agency thereof. The views and opinions of authors expressed herein do not necessarily state or reflect those of the United States Government or any agency thereof.

## SPECTROSCOPIC PROPERTIES OF THE f-ELEMENTS IN COMPOUNDS AND SOLUTIONS

W. T. Carnall, J. V. Beitz, H. Crosswhite

Chemistry Division, Argonne National Laboratory,  
9700 South Cass Avenue, Argonne, Illinois 60439

K. Rajnak

Physics Department, Kalamazoo College,  
Kalamazoo, Michigan 49007

J. B. Mann

Los Alamos National Laboratory, Los Alamos,  
New Mexico 87545

### ABSTRACT

In this systematic examination of some of the spectroscopic properties of the f-elements we deal with both the trivalent lanthanides and actinides. We summarize the present status of our energy level calculations in single crystal matrices and in aqueous solution, and compare the predicted crystal-field structure in certain low-symmetry sites with that observed. Some interesting new structural insights are thereby gained. The state eigenvectors from these calculations are then used in part in reassessing and interpreting the intensities of transitions in aqueous solution via the Judd-Ofelt theory. The parameters of this theory derived from fitting experimental data are compared with those computed from model considerations. Finally, we discuss some recent contributions to the interpretation of excited state relaxation processes in aqueous solution.

The submitted manuscript has been authored by a contractor of the U.S. Government under contract No. W-31-109-ENG-38. Accordingly, the U.S. Government retains a nonexclusive, royalty-free license to publish or reproduce the published form of this contribution, or allow others to do so, for U.S. Government purposes.

MASTER

E&B

## I. SYSTEMATIC ANALYSIS OF THE ENERGIES OF LANTHANIDE TRANSITIONS IN SOLIDS AND IN AQUEOUS SOLUTION

In this section we begin with a brief summary of the theoretical models used to compute the energy level structure within the  $f^N$ -configurations of the trivalent lanthanides (Ln) and actinides (An). The discussion focuses on relating observed absorption band structure, interpreted in terms of transitions within the  $f^N$ -configuration, to the complete set of energy levels for the configuration. The interpretations in subsequent sections all depend directly on the ability to model the interactions that give rise to the electronic structure. The purpose of the summary is not only to give a status report on an area that is still under development but to try to indicate the extent to which the models are sensitive to apparent changes in the observed spectra.

### I(A). Model Interactions for $f^N$ -Configurations

The process of developing a complete Hamiltonian for  $f^N$ -configurations is approached in stages. The first deals with the energy level structure of the gaseous free-ion, and the second with the additional (crystal-field) interactions which arise when the ion is in a condensed phase. The free-ion Hamiltonian is assumed to be the same in both cases, and the centers of gravity of groups of crystal field levels are interpreted on the same basis as the degenerate levels of the gaseous free ion. Because of the abundance of data in condensed media, and the paucity of true gaseous free ion data, the Hamiltonian for the ion in condensed phases has been much more extensively studied. Thus, unless explicitly noted, subsequent data on the "free ion" Hamiltonian will refer to studies of ions in condensed media.

The fundamental interactions that give rise to the free-ion structure in trivalent lanthanides and actinides are the electrostatic repulsion between electrons in the  $f^N$ -configuration and the coupling of their spin and orbital angular momenta. For details of the development see [1-4]. There are two different approaches to modeling these types of interaction--the Hartree-Fock (HF) approach and what we will call the Parametric approach. Both begin with Schrödinger equation for the steady state of a many electron system, Fig. I-1.

The actual form of the Hamiltonian assumes that the nucleus can be treated as a point charge with infinite mass. Since exact solutions are only known in the one-electron case, some method of approximation must be used. In both the HF and parametric approaches, the first step is to obtain approximate total wavefunctions based on the central field approximation. Each electron is assumed to move independently in the field of the nucleus and a central field composed of the spherically averaged potential

fields of each of the other electrons in the system. In other words, each electron is treated as if it moved independently in a spherically symmetric potential.

The HF-approach seeks the evaluation of this potential using the variational principle [5]. Computed values of the desired integrals can be obtained to varying degrees of approximation depending upon the sophistication of the computer codes used. The effects of configuration interaction can in principle be introduced, but in practice this is normally not done.

In the parametric approach, each electron is assumed to move in a central field satisfying an equation similar to the Schrödinger equation for the hydrogen atom, except that the Coulomb potential  $-e^2/r$  is replaced by an undefined central field potential  $U(r)$ . Variables are separated as with the hydrogen atom, and the angular parts of the interaction are evaluated explicitly. Since the radial equation contains the undefined function,  $U(r)$ , it cannot be solved. The radial integrals are treated as parameters to be evaluated from experimental data via an appropriate fitting procedure. The expression for the energy, Fig. I-2, has the same form as that of the HF-approach, but there is no radial function from which to evaluate the  $F^k$  and  $\zeta$ .

The parametric method can be extended to include the effects of configuration interaction by the use of perturbation theory. If it is assumed that the difference in energy between all perturbing configurations,  $E(P)$ , and the  $f^N$ -configuration,  $E(f^N)$ , is very large such that  $\Delta E = E(P) - E(f^N)$  is effectively constant, then the closure theorem is valid and the effects of configuration interaction can be represented by certain operators acting within the  $f^N$  configuration. These result in

1. changes in the original  $F^k$
2. additional 2- and 3-body (effective) operators operating within the  $f^N$ -configuration

Within the above context, the new  $F^k$  integrals should not be identified as the integrals of the HF model but as parameters that absorb some of the effects of configuration interaction. For further discussion and references see [6,7].

Model calculations which include only the electrostatic interaction in terms of the  $F^k$ -integrals, and the spin-orbit interaction,  $\zeta$ , result in correlations between calculated and observed gaseous free-ion states that are only marginally useful. It was pointed out some 40 years ago, for example, that in the relatively simple cases of  $Pr^{3+}$  and  $Tm^{3+}$  ( $4f^2$  and  $4f^{12}$ ) differences

between calculated and observed energy levels were in some cases  $>500 \text{ cm}^{-1}$  [8]. A poor correlation of this magnitude severely limits the usefulness of the calculations for analyzing data [9].

The two-body effective operator correction terms incorporated into systematic parameter evaluations for the lanthanides to account for the effects of configuration interaction are usually expressed in the form given by Rajnak and Wybourne [10]. The principal terms of the Hamiltonian including the two-body (scalar) operators for configuration interaction can be written:

$$H = \sum_{k=0}^{6} F^k (nf, nf) f_k + \zeta_f A_{SO} + \alpha L(L+1) + \beta G(G_2) + \gamma G(R_7) \quad (k \text{ even}) \quad (I-1)$$

where  $f_k$  and  $A_{SO}$  represent the angular parts of the electrostatic and spin-orbit interactions, respectively. Similarly  $\alpha$ ,  $\beta$ , and  $\gamma$  are the parameters of the two-body correction terms while  $G(G_2)$  and  $G(R_7)$  are Casimir's operators for the groups  $G_2$  and  $R_7$ . The effects of configuration interaction that can be expressed in the same form as the  $f_k$  are of course automatically absorbed in the  $F^k$  radial integrals when they are treated as parameters. The additional terms,  $\alpha$ ,  $\beta$ , and  $\gamma$  thus represent effects that do not transform as the  $f_k$ .

The values of  $\alpha$ ,  $\beta$ , and  $\gamma$  arising from electrostatic configuration interaction have been calculated for  $\text{Pr}^{3+}$  by Morrison and Rajnak [11], using *ab initio* methods, Table I-1. A particularly useful insight gained from this work was that higher energy processes such as excitation of one or two particles to the continuum made large contributions to the parameter values. The fact that the energies of the continuum states relative to the  $f^N$ -configurations did not change significantly with atomic number could be correlated with the near constancy of the fitted parameter values across the lanthanides series [12,13]. A subsequent perturbed-function approach to the calculation of the same continuum interactions addressed in [11] confirmed the results for  $\text{Pr}^{3+}$  and extended the calculation to other 3+ lanthanides as well as to  $\text{Pu}^{3+}$  [14].

For configurations of three or more equivalent f electrons, three-particle configuration interaction terms have been added to the model in the form given by Judd [15] and Crosswhite *et al.* [16], Table I-1. Such terms arise from the perturbing effects of those configurations that differ from  $f^N$  in the quantum numbers of a single electron, and are expressed as  $T_i t_i$  ( $i = 2, 3, 4, 6, 7, 8$ ) where  $T_i$  are the parameters and  $t_i$  are matrix elements of

three-particle operators within the  $f^N$  configuration. As in the case of the two-body terms, values of the three-particle correction parameters have been calculated by *ab initio* methods and found to agree with those defined by fitting experimental data, Balasubramanian *et al.* [17]. The values of these parameters have also been shown to be nearly constant over the lanthanide series.

Magnetically correlated corrections to the interactions included in Eq. I-1 have been introduced in the form suggested by Judd *et al.* [18]. Values of the Marvin integrals,  $M^h$  ( $h = 0, 2, 4$ ), which represent spin-spin and spin-other-orbit relativistic corrections, were initially determined from parametric fits to experimental data. However, the values obtained were essentially identical to those computed using HF-methods, so that more recently the latter values either have been used directly and not optimized, or  $M^0$  has been varied while  $M^2$  and  $M^4$  were fixed in their HF ratios to  $M^0$ . The two-body magnetic corrections,  $a_{ij}z_i$ , appear to be dominated by the electrostatically correlated spin-orbit perturbation which involves the excitation of an  $f$  electron into a higher-lying  $f$ -shell. The corresponding parameters  $p_f$  ( $f = 2, 4, 6$ ) show a regular increase across the lanthanide series, but have exclusively been evaluated by parametric fitting [12].

Although extensive corrections to the free-ion Hamiltonian have been developed, practically all crystal-field calculations are carried out using a single-particle crystal-field theory in which the parameters are appropriate to a given site symmetry,  $H_{CF} = \sum_{k,q,i} B_q^{(k)} (C_q^{(k)})_i$ . For details and references to the original literature see [1-3]. Thus to complete the interactions given in Eq. I-1, the following terms are included in the Hamiltonian currently used in the parametric fitting of the experimental data:

$$\sum_{i=2,3,4,6,7,8} T_i^i t_i + \sum_{k=0,2,4} M^h m_h + \sum_{f=2,4,6} p_f^f p_f + \sum_{k,q} B_q^k C_q^{(k)}$$

Typical values of the atomic parameters appropriate to  $\text{Nd}^{3+} : \text{LaCl}_3$  [19], are included in Table I-1.

### I(B). Interpretation of the Model Parameter Values

Hartree-fock values of the  $F^k$ 's and  $\zeta_f$  are always larger than those obtained by allowing them to vary as parameters. There are several reasons for this:

- 1) The usual HF-calculation is non-relativistic; inclusion of relativistic effects can improve the agreement with experiment, but discrepancies remain. The HFR code of Cowan and Griffin [20], has the advantage of nearly reproducing the relativistic results, via a pseudorelativistic correction to the potential, while maintaining the simpler non-relativistic formalism. It gives remarkably good agreement with empirical values of  $\zeta$  but the  $F^k$ 's, while smaller than HF values, remain considerably larger than the empirical ones, (Table I-1). This indicates that differences between HF and empirical  $\zeta$  values arise largely from neglect of relativistic effects. There is also a relativistic effect on the  $F^k$ 's but that is not the major consideration.
- 2) Even a relativistic HF calculation is usually based on interactions in a pure  $f^N$ -configuration whereas the f-electrons spend some time in higher-lying configurations where they move in larger orbits and interact less than the *ab initio* model assumes. In addition, the experimental results are frequently for an ion in a condensed phase, not for a gaseous free-ion. However, this effect is not very large. The value of  $F^2$  for Pr(IV) free-ion is only  $\sim 6\%$  larger than that for  $\text{Pr}^{3+}:\text{LaCl}_3$ , Table I-2 [21].

While the HFR values of  $F^k$  are too large, the differences between the HFR and the experimental (parametrized) values,  $F^k(\text{HFR}) - F^k(\text{EXP}) = \Delta F^k$ , have been shown to be nearly constant over the lanthanide series, as illustrated in Figs. I-3 and I-4 [12]. Both  $\zeta_{4f}$  and  $F^2$  vs.  $Z$  change slope at  $Z = 64$  ( $\text{Gd}^{3+}$ ), Figs. I-3 and I-5. While fitting of data near the center of the series poses special problems, the parametric fit results appear to be consistent with HFR calculations. Similar results have been obtained with the actinides [13].

### I(C). Crystal-Field Calculations

Having defined the atomic (or free-ion) portion of the parametric model, and indicated that consistent results are obtained using it over both the lanthanide and actinide series, we will briefly address the status of crystal-field calculations and some problems that have arisen as better correlation with experiment has been achieved. Judd [22,23] has recently drawn attention to some of the inadequacies of the single-particle model currently in use, and has suggested refinements. However, the following discussion deals with the general conception of the model.

As Wybourne [1] pointed out, the crystal field was originally thought of as a purely electrostatic interaction between the central ion and the surrounding ligands with the latter replaced by point charges. A more general approach considers the potential energy  $V(r)$  of an electron of a central ion where  $r$  is the radius associated with an f-electron. The environment is then represented by a classical charge distribution  $\rho(R)$  where  $R$  is the radius associated with a general point in that environment:

$$V(r) = - \int \frac{e \rho(R) dr}{|R-r|} \quad (I-2)$$

When this potential is expanded in terms of Legendre polynomials and the spherical harmonic addition theorem applied, the result can be written

$$V(r) = \sum_{k,q} B_q^k C_q^{(k)} \quad (I-3)$$

$$B_q^k = e \int \rho(R) \frac{r_-^k}{r_+^{k+1}} (-1)^q C_{-q}^{(k)} (\theta, \phi) d\tau \quad (I-4)$$

$$= \langle r^k \rangle \left[ -e \int_R \frac{\rho(R)}{R^{k+1}} (-1)^q C_{-q}^{(k)} (\theta, \phi) d\tau \right] \quad (I-5)$$

The expression given in Eq. (I-3) is the usual form of the crystal-field potential where  $B_q^k$  are the parameters and  $C_q^{(k)}$  are tensor operators which represent the angular part of the crystal field interaction. The values of  $k$  and  $q$  for which the  $B_q^k$  are non-zero are determined by the symmetry of the crystal field. Hüfner [3] pointed out in his recent book that, whereas the aspect of crystal field splitting that is symmetry related is well understood, the mechanisms that determine the magnitude of the splitting are "by no means completely understood".

In obtaining a fit to experimental crystal field levels we use Eq. (I-3), treating the  $B_q^k$  as parameters. Since complete atomic and crystal field matrices can now be diagonalized simultaneously, we allow for J-mixing, but we have not introduced any corrections to the single particle crystal-field model. Parametrization of the crystal field has been extremely successful in correlating a large amount of the data, particularly with the  $\text{Ln}^{3+}:\text{LaCl}_3$  system where the data base includes polarization and Zeeman effect measurements [12].

The free-ion and crystal-field parameters for a well characterized system,  $\text{Nd}^{3+}:\text{LaCl}_3$  are shown in Table I-3. The complete model parameters are indicated in column C, and they reproduce 101 experimentally verified levels (i.e., polarization and Zeeman spectra were also taken) of the total set of 182 with a root mean square deviation of  $8.1 \text{ cm}^{-1}$  [19]. In column B the free-ion parameter set was reduced to include only the two-body configuration interaction operators. As a result the parameter values are distorted compared to those in Column C as they rather unsuccessfully attempt to fit the same 101 crystal-field components. The crystal-field interaction in lanthanide spectra can usually be treated as a perturbation and consequently even early attempts to define the parameters were successful if the energies of the crystal field components for a given state were arbitrarily adjusted to fit the centers of gravity of the observed free-ion groups (Column A). For the experimentalist, the significance of the refined model is clear. It is a working tool. It provides the basis for predicting the energies of crystal-field components in unanalyzed regions of the spectrum, sometimes calling attention to very weak features of the spectrum. The error in the predicted energy is expected to be small in comparison to the usual energy separation of crystal-field components.

Attempts to calculate the crystal-field parameters from first principles are still in progress. The early work of Hutchings and Ray [24], which explored and indicated the limitations of the point charge model, and more recent work by Faucher *et al.* [25] can be contrasted with attempts of other groups, particularly Newman and coworkers, who have expressed their results in terms of the angular overlap and covalency contributions to the crystal-field parameters [26-28]; comparisons are shown in Fig. I-6.

In the following section we focus on some new insights into both the symmetry and the magnitude of the crystal field. The expression given in Eq. (I-4) is general. If  $r_{\zeta}^k$  is associated with an f-orbital and  $r_{\zeta}^{k+l}$  with R, then integration over the f-electron wave function gives the expectation value,  $\langle r^n \rangle$ , and its coefficient is the potential due to the ligands. Energy level analyses of  $\text{U}^{3+}:\text{LaCl}_3$  [29] and  $\text{Np}^{3+}:\text{LaCl}_3(\text{LaBr}_3)$  [7] were recently published. The values of  $P_{\zeta}^k$  were approximately twice the magnitude of corresponding values for the lanthanides. The question that arises is whether this increased magnitude is consistent with, larger than, or smaller than expectations.

The literature contains a number of examples of HF-calculations which indicate that the 5f-orbitals are less well shielded by filled s and p shells than is the case for lanthanides. In Fig. I-7 the results of calculations using an HFR program are

shown with the 4f and 5f vertical scales increased relative to those of the cores [29]. For  $\text{Nd}^{3+}$ , the radius corresponding to the maximum in the probability function ( $r^2\psi^2$ ) for the 4f electrons is well inside that for the 5s and 5p electrons. In contrast the probability function maxima for the 5f, 6s, and 6p electrons all occur at essentially the same radius.

We were interested in determining whether the factor of two difference in magnitude of the crystal field parameters for  $\text{Ar}^{3+}:\text{LaCl}_3$  compared to  $\text{Ln}^{3+}:\text{LaCl}_3$  could be correlated with the apparent increased potential for overlap between the 5f and ligand wavefunctions. A purely electrostatic point of view, the point charge model, was adopted [7]. Since values of  $\langle r^k \rangle$ , Eq. (I-5), have been computed (both with relativistic and non-relativistic codes), and since the crystal-field parameters of both  $\text{Np}^{3+}$  and the lanthanide analog have been determined from spectra in the  $\text{LaCl}_3$  host, we argued that to a first approximation the terms from Eq. (I-5) which involve the crystal host would cancel, giving the expression:

$$\frac{\langle r^k \rangle}{B_q^k(\text{An}^{3+} \text{ predicted})} = \frac{\text{An}^{3+}}{\langle r^k \rangle_{\text{Ln}^{3+}}} B_q^k(\text{Ln}^{3+}) \quad (\text{I-6})$$

Results using Eq. (I-6) are shown in Table I-4. If we use values of  $\langle r^k \rangle$  computed with a non-relativistic rather than a relativistic HF code, the values of the scaled parameters are in better agreement with those obtained by fitting experimental data. We took the foregoing as evidence that the magnitude of the crystal field parameters in  $\text{Np}^{3+}$  compared to  $\text{Pm}^{3+}$  could indeed be rationalized solely on the basis of electrostatic considerations. From this point of view, the increased potential for overlap between f and ligand orbitals, indicated in Fig. I-7 for a 5f compared to a 4f species, a covalency effect, could not be identified as the source of the increase in parameter values.

Poon and Newman [30] took exception to the underlying assumption that the lanthanide crystal-field was primarily electrostatic in character and that the suggested mode of scaling might reveal pronounced covalency in the actinides. They pointed out that based on the superposition model, overlap and covalency represent the major contributions to the crystal field in the lanthanides. The considerable overlap between 4f and  $\text{Cl}^-$  wavefunctions in  $\text{PrCl}_3$  had actually been indicated in the earlier HF-calculations reported by Hutchings and Ray [24]. If one accepts this argument, then it would certainly be reasonable to assume that the same interactions predominate for the actinides. Poon and Newman showed

that it is possible to develop an expression which is the analog of Eq. (I-6) with the  $\langle r^k \rangle$  replaced by overlap integrals between  $\text{Cl}^-$  and the metal centers. Using the value  $d = 2.94 \text{ \AA}$ , characteristic of the  $\text{Np}^{3+} - 6\text{Cl}^-$  bond distance, the ratio is essentially identical to that for  $\langle r^k \rangle_{5f} / \langle r^k \rangle_{4f}$ .

It appears, therefore, that both "models" are consistent with the changes in magnitude of the crystal-field parameters defined by experiment. However, it is also possible to rationalize the two seemingly different approaches. From the ionic point of view, there is no evidence of a disproportionate increase in the role of covalency when comparing the  $\text{An}^{3+}$  and  $\text{Ln}^{3+}$  crystal-field parameters. From the viewpoint advanced by Poon and Newman, the increased overlap between metal and  $\text{Cl}^-$  centers, and the increased magnitude of the crystal field parameters are mutually consistent. From the latter standpoint, Fig. I-7 may tend to suggest a greater potential for radial overlap in  $\text{An}^{3+}$  compared to  $\text{Ln}^{3+}$  than is actually borne out by the present experiment. Nevertheless, the increase in covalency is not to be considered disproportionate. It is perfectly consistent with expectations.

#### I(D). Approximate Symmetries

We have carried out calculations of the crystal-field parameters with the usual assumption that the symmetry-related dependence of the field, the  $C_d^{(k)}$  operators in Eq. (I-3), is well understood. However there are aspects of this part of the treatment that are difficult to define. For example, there are many crystal lattices in which the central ion ( $\text{Ln}^{3+}$  or  $\text{An}^{3+}$ ) resides at a low symmetry site. We are very much interested in exploring the circumstances under which it is appropriate to adopt a higher, more mathematically tractable, approximate symmetry for such cases that would allow computation of crystal-field levels in good agreement with those observed experimentally.

Some useful insights into the problem have been derived from recent analyses of the spectra of  $\text{Ln}^{3+}:\text{LaF}_3$ . The actual site symmetry in  $\text{LaF}_3$  is  $C_2$  [31, 32] but the approximate symmetry approaches that of  $\text{LaCl}_3$  ( $D_{3h}$ ) [33]. As a point of reference, the crystal-field analysis of  $\text{Nd}^{3+}:\text{LaCl}_3$ , Table I-3, is a good example of the degree to which the present model can reproduce experimental data taken in a well characterized lattice over a broad range of the optical spectrum.

It was pointed out by Onopko [34] that the energies of the crystal-field components of several of the lowest-lying free-ion states in  $\text{Nd}^{3+}:\text{LaF}_3$  and  $\text{Er}^{3+}:\text{LaF}_3$  could be computed in reasonable agreement with experiment by assuming that the site symmetry approached  $D_{3h}$ . A point charge calculation confirmed the signs of

the parameters shown in Table I-5, as did a molecular orbital treatment carried out by Newman and Curtis [35]. A subsequent analysis based on Onopko's crystal-field parameters and reasonable sets of free-ion parameters, showed that the energies of crystal-field transitions in  $\text{Nd}^{3+}$ ,  $\text{Sm}^{3+}$ ,  $\text{Gd}^{3+}$ ,  $\text{Dy}^{3+}$ , and  $\text{Er}^{3+}$ , each doped into single crystal  $\text{LaF}_3$ , could be calculated in good agreement with experiment over the whole of the optical range to  $50000 \text{ cm}^{-1}$  [36]. As indicated in Table I-5, the deviations between calculated and assigned energy levels for the  $\text{Ln}^{3+}:\text{LaF}_3$  spectra were exceedingly small and compared well with those for the  $\text{LaCl}_3$  host.

In the 3+ lanthanides with an odd number of f-electrons, the crystal-field will induce a splitting of each free-ion state into  $J+1/2$ -components in all site symmetries except cubic or  $D_h$ . Thus the number of components is the same for  $C_2$  as for  $D_{3h}$ . On the contrary, in even f-electron systems such as the oft studied  $\text{Pr}^{3+}:\text{LaF}_3$ , ( $4f^2$ ), crystal-field calculations in  $D_{3h}$  symmetry do not remove the degeneracy of the  $\mu = +1$  or  $\mu = +2$  states, yet the number of lines observed in the spectrum of  $\text{Pr}^{3+}:\text{LaF}_3$  does imply a lower site symmetry consistent with the complete removal of symmetry-related degeneracy. Thus analysis of the crystal-field in even f-electron systems was not attempted when using the  $D_{3h}$  approximation [36].

Subsequently Morrison and Leavitt [37] published an analysis of the spectra of  $\text{Ln}^{3+}:\text{LaF}_3$  using the actual  $C_2$  symmetry crystal-field. Initial values of the 14 crystal-field parameters for ions with an odd number of f electrons were obtained from lattice sum calculations referred to a coordinate system in which the crystal axis was parallel to the  $C_2$ -axis and perpendicular to that in  $D_{3h}$ -symmetry. For practical computational reasons, they adopted a modified free-ion Hamiltonian which allowed adjustment of the centroids of the crystal-field levels associated with a given free-ion state so as to maximize the fitting of experimentally established sets of crystal-field components. Only the 9-10 lowest energy multiplets of ions with odd numbers of f-electrons were involved in the fitting process. These results provided the initial parameters used in the present fitting of even f-electron cases. The magnitudes of crystal-field parameters relevant to this study are indicated in Table I-6.

The calculation in  $C_2$ -symmetry requires determination of 14 independent crystal-field parameters, and this is a major computational problem, particularly when coupled with the extensive free-ion treatment. We therefore sought a middle ground by exploring the possibility of using an approximate  $C_{2v}$ -symmetry, which is low enough to completely remove the symmetry-required degeneracy of crystal-field states, yet allowed us to retain the

extensive free-ion model and to continue to simultaneously diagonalize the atomic and crystal field portions of the Hamiltonians.

There are at least two approaches to use the  $C_{2v}$  approximation. One is to maintain the  $D_{3h}$  symmetry axis and add the additional parameters introduced in the  $C_{2v}$  case to simulate the distortion from  $D_{3h}$  symmetry. This was the original course we chose, since by fitting an odd-f electron case in this manner, the extra parameters could be determined and subsequently used as a trial set to interpret the spectra of even f-electron spectra. One of the problems encountered is that the  $D_{3h}$  approximation provides such a good correlation between experiment and theory that it is difficult to adequately determine the extra parameters arising in the  $C_{2v}$  symmetry so that their magnitude and signs may be arbitrary, depending upon the data being fit. This approach has been discussed by Caro and coworkers [38].

The other approach is to fit the crystal-field states of an odd f-electron system using as an initial set of parameters either the real part of the set computed for  $\text{LaF}_3$  in  $C_2$ -symmetry ( $C_2$ -axis) [37] or a set derived from the  $D_{3h}$ -approximation of the  $\text{LaF}_3$  structure ( $D_{3h}$ -axis) transformed by a suitable rotation of axes. The experimental data for  $\text{Er}^{3+}:\text{LaF}_3$  are particularly useful for testing such parametrization methods, because practically all of the crystal-field states to  $\sim 40000 \text{ cm}^{-1}$  have been assigned [36]. A comparison of different sets of crystal-field parameters fit to  $\text{Er}^{3+}:\text{LaF}_3$  data is shown in Table I-7. There is little change in the values of  $B_2^2$ ,  $B_4^4$ ,  $B_6^6$  and  $B_6^6$  between the  $D_{3h}$  case and the  $C_{2v}$  set ( $D_{3h}$ -axis). However starting from the  $C_2$ -parameters ( $C_2$ -axis) obtained by Morrison and Leavitt in a limited fit to  $\text{Er}^{3+}:\text{LaF}_3$  data, it is apparent that a final set can be derived ( $C_2$ -axis) in which the parameters themselves are better determined.

A reasonable test of the  $C_{2v}$  approximation would involve its application to even f-electron systems. Thus we have combined the crystal field parameters shown in Table I-7 ( $C_{2v}$ - $C_2$  axis) for  $\text{Er}^{3+}:\text{LaF}_3$  with a set of free-ion parameters for neighboring  $\text{Ho}^{3+}$  derived from a fit to the approximate centers of gravity of observed crystal-field components, but also constrained to be consistent with the trends observed in similar parameters for other  $\text{Ln}^{3+}:\text{LaF}_3$  [36]. Diagonalization of the combined set provided a model calculation with which observed structure in  $\text{Ho}^{3+}:\text{LaF}_3$  could be compared. Much of the multiplet structure was very satisfactorily fit; however, some useful insights were immediately gained. The experimental results for the  $5I_7$ -state [39], are compared with the computed structure of that state in Fig. I-8.

There are several features of the figure that make it a good example of the importance of the interaction between theory and

experiment. Considering the left side of Fig. I-8 (larger range of energies) it is apparent that the calculated crystal-field components are grouped from  $\sim 5200$ - $5300 \text{ cm}^{-1}$  and there is no computed analog for levels  $Y_{11}$ - $Y_{15}$ . These were levels that were relatively poorly resolved and only observed in fluorescence; however, there was no experimental basis for excluding them. It was noted that some of the levels might be vibronic in origin. The present computed set would have been extremely helpful in encouraging the experimentalist to look for a possible assignment to another group. On the right side of Fig. I-8 the crystal-field structures computed assuming  $C_{2v}$  ( $C_2$ -axis) and  $D_{3h}$  symmetries are compared using an expanded energy scale. The fundamental grouping of levels is reproduced by the approximate  $D_{3h}$ -symmetry. Recourse to  $C_{2v}$ -symmetry removes the degeneracy of several levels consistent with experiment, but it also indicates the energy range in which additional structure should be observed. While assignments can be made based on the model calculation, significant improvement of the fit would not be expected because of the very small adjustments required. The spectrum of the  $^5I_7$  group at  $\sim 4^\circ\text{K}$  is shown in Fig. I-9. Some of the indicated structural features may be vibronic in character, so that in general the model predictions will also be of value in avoiding assignment to some relatively prominent structure of that possible origin. The advantages of the interaction of the type of model calculation discussed here with experimental data is apparent. However one of the deficiencies of the present analysis is a further independent method (other than corresponding energies) for assigning crystal-field components in  $\text{La}^{3+}:\text{LaF}_3$ . The attempts to compute crystal-field component intensities based on model calculations is one important new direction [40], another is to examine the correlation between observed magnetic properties and values calculated from crystal-field eigenvectors [38].

## II. THE INTENSITIES OF $f \rightarrow f$ TRANSITIONS IN ABSORPTION AND IN FLUORESCENCE

The use of absorption spectra to monitor changes in the environment of transition-metal ions is a widely applied technique. The normally sharp well-defined absorption bands characteristic of the trivalent lanthanides and actinides, are particularly useful in this respect. Moreover, while shifts in band energies and intensities can be a qualitative indicator of environmental changes, it was realized in the 1930's and 40's that spectra of the  $f$ -elements could in principle be subjected to a detailed intensity analysis if the knowledge of their energy level structures in various media were sufficiently detailed. Such an analysis would require some modeling of the ionic environment.

In the early 1940's a group of Dutch scientists [41] carried out the first comprehensive quantitative study of the intensities of rare earth absorption bands in solution. They measured the area under the band envelopes for solutions of known concentration and thereby established values for the oscillator strengths,  $P$ , of various transitions:

$$P = \frac{2303 \frac{mc}{N\pi e}^2}{\lambda^2} \int \epsilon_i(\sigma) d\sigma = 4.32 \times 10^{-9} \int \epsilon_i(\sigma) d\sigma \quad (\text{II-1})$$

where  $\epsilon = \frac{1}{C\lambda} \log \frac{I_0}{I}$ ;  $C$  is the molar concentration of the f-element,  $\lambda$  is the light path in the solution (cm), and  $\log \frac{I_0}{I}$  is the absorptivity at a given energy  $\sigma$  ( $\text{cm}^{-1}$ ) within the band envelope.

The general form of the theoretical model for the oscillator strength of a transition corresponding to Eq. II-1 was written [41],

$$P = \frac{8 \frac{\pi^2}{3} \frac{mc\sigma}{\lambda^2}}{(2J+1)} \left[ \chi \bar{F}^2 + n \bar{M}^2 \right] \quad (\text{II-2})$$

where  $\chi = \frac{(n^2+2)^2}{9n}$  is the refractive index ( $n$ ) correction, and  $\bar{F}^2$  and  $\bar{M}^2$  are respectively the matrix elements of the electric dipole and magnetic dipole operators between the ground state and a particular excited state. The problem was to be able to calculate the required matrix elements for transitions of interest.

Practically all of the lanthanide absorption bands usually observed in the near-infrared to near-ultraviolet range of the spectrum are attributed to electric dipole transitions, although in the strict sense such transitions are parity forbidden since they occur between states within the same configuration. The intensities of lanthanide transitions, which result in bands with  $P \sim 10^{-6}$ , indeed reflect a highly forbidden character compared to allowed transitions (such as  $f \rightarrow d$ ) where  $P = \sim 1$ . However, it was pointed out by Broer *et al.* [41], based on earlier work of van Vleck [42] that the observed intensities could be accounted for by assuming a small mixing of the higher-lying opposite parity configurations, i.e.  $f^N \rightarrow f^{N-1}d$ ,  $f^{N-1}g$ , and others into the  $f^N$ -states via the odd terms in the potential due to the ligand field.

The work of Broer and coworkers was based on the analysis of aqueous solution spectra. While of considerable interest in its

own right, this medium has obvious experimental advantages, including the assurance of homogeneity of lanthanide distribution. A number of analyses of the spectra of lanthanides either neat or doped into crystal hosts have by now also been published.

While the character of the  $f^N$ -transitions had been established prior to 1962, the problem of computing the matrix elements of  $F$  (Eq. II-2) for lanthanide ions in an arbitrary crystal or ligand-field environment had not been fully addressed. On the other hand, computation of the matrix elements of  $M$ , the magnetic dipole operator between the ground state and any given excited state was well understood. For a summary of the method see [43]. Very few of the observed transitions exhibit any appreciable magnetic dipole character.

Thus in 1962 when Judd [44] and independently Olfelt [45] derived closed expressions for  $F^2$  they opened the way for a new dimension in the analysis of rare earth absorption spectra. At about the same time, the early 1960's, there developed a very active interest in the mechanisms of excited state relaxation of rare earths both in solutions and in crystals. As the analysis proceeded, it was shown that the Judd-Olfelt theory could be used to compute the total radiative relaxation rates of excited states of interest. This made it possible to predict pathways of excited state relaxation; although, most states were found to relax primarily via non-radiative mechanisms. In recent years, a new field of rare earth laser engineering has emerged to identify potential lasing transitions for rare earths in various host crystals. Concepts evolved in use of the Judd-Olfelt theory are also applicable to the screening of rare earth doped glasses to maximize the efficiency of high power lasers for use in both fusion and fission energy applications [46,47].

At this point, 20 years after publication of the Judd-Olfelt theory, we recall particularly its successful use in extending our knowledge of the energy level schemes of the lanthanides, and its contribution to the study of excited state relaxation [48]. In this section we reexamine and extend our previous efforts to understand the intensity patterns exhibited by lanthanide transitions in solution, and project the discussion to the trivalent actinides where new analyses have been carried out. A knowledge of the energy level structure which allows identification of transitions observed in solution in terms of a useful coupling scheme is the basis for the intensity analysis. Consequently, the results of the energy level analysis of systems such as  $\text{Ln}^{3+}:\text{LaF}_3$  are directly applicable to the developments discussed here.

## II(A). Judd-Ofelt Theory

In effect, the efforts to interpret rare earth solution spectra prior to 1962 had established that:

$$P_{\text{EXPT}} = P_{\text{ED}} + P_{\text{MD}}$$

that is, an experimentally measured quantity, the oscillator strength (or probability for absorption of radiant energy) could be expressed to a good approximation in terms of absorption of light by electric and magnetic dipole mechanisms without recourse to higher multipoles.  $P_{\text{MD}}$  was known to be important in only a few transitions, so principal interest focused on  $P_{\text{ED}}$ .

Judd derived the expression [44]:

$$P_{\text{ED}} = \sum_{\lambda=2,4,6} T_{\lambda} \nu (\psi J || U^{(\lambda)} || \psi' J')^2 \quad (\text{II-3})$$

where  $\nu(\text{sec}^{-1})$  is the frequency of the transition  $\psi J \rightarrow \psi' J'$ ,  $U^{(\lambda)}$  is a tensor operator of rank  $\lambda$ , and the  $T_{\lambda}$  are quantities which contain the description of the immediate environment of the rare earth ion as well as overlap integrals and energy differences. The beauty of this result was that Judd was able to substitute three parameters,  $T_{\lambda}$ , for those interactions that constitute the model of the ion in its environment. Since the matrix elements of  $U^{(\lambda)}$  could be calculated from a knowledge of the free-ion structure of the ion of interest, the parameters could be determined empirically from experimental data.

$$T_{\lambda} = \frac{8\pi^2 m}{3h} \frac{\lambda}{2\lambda+1} (2\lambda+1) \sum_t (2t+1) B_t \Xi^2(t, \lambda) \quad (\text{II-4})$$

- $B_t = \sum_p |A_{tp}|^2 / (2t+1)^2$  expresses the influence of the environment on the central ion. The  $A_{tp}$  are the odd components of the crystal field.
- $\Xi^2(t, \lambda) = f [(n1) |r| (n'1') (n1 | r^t | n'1') / \Delta n'1']$  involves radial integrals coupling the  $f^N$  to perturbing configurations and energy differences.

Since  $T_\lambda$  is composed of several parts, it is difficult to extract explicit information about the environment. The problem is similar to that met in crystal-field calculations. The parametrization in terms of  $U(\lambda)$  does not imply a unique model.

A useful alternate parametrization of Judd's expression [48], is adopted here and written:

$$P_{ED} = \frac{8\pi^2 mc}{3h} \frac{\sigma}{(2J+1)} \times \sum_{\lambda=2,4,6} \Omega_\lambda \langle \psi_J | |U^{(\lambda)}| | \psi'_{J'} \rangle^2 \quad (II-5)$$

The values of Judd's  $T_\lambda$  and  $\Omega_\lambda$  defined above are related by  $\Omega_\lambda = (2J+1) [3.618\chi]^{-1} T_\lambda$  (for transition frequency in  $\text{sec}^{-1}$ ). Most experimental results are now quoted in terms of the energy in  $\text{cm}^{-1}$  of the transitions. When this framework is used the appropriate conversion factor is  $\Omega_\lambda = (2J+1) [1.085 \times 10^{11} \chi]^{-1} T_\lambda$ . The rationale for modifying Judd's original notation and adopting that of Eq. II-5 is that the latter is more directly related to the subsequent calculation of intensities in emission.

In our original use of the Judd-Ofelt theory [49], we showed that a single set of three parameters could reproduce the observed intensities of all the absorption bands for a given  $\text{Ln}^{3+}(\text{aq})$  ion, within a reasonable degree of accuracy. However, in the early stages of this work our understanding of the energy level schemes was fragmentary, particularly the structure at higher energies. Thus as soon as the Judd-Ofelt theory had been tested and shown to be capable of reproducing the intensities of well characterized lower-energy absorption bands, it was realized that the theory could also be utilized as a basis for identifying the transitions involved in isolated, more intense absorption bands at higher energies. With the resulting new assignments it was possible to explore the parametrization of configuration interaction in  $f^N$ -configurations in a much broader and more systematic manner than had previously been attempted.

There were of course limitations on the extent to which even the improved parameterization scheme could represent the data. Subsequent developments have culminated in the extensive analysis of energy level structure in lanthanide spectra discussed in section I. At this point it is of some interest to return to the analysis of intensities for  $\text{Ln}^{3+}(\text{aq})$  and reexamine the intensity parameters which can now be derived based on an independent and consistent analysis of the energy level structure. Inspection shows that the free-ion states computed for  $\text{Ln}^{3+}:\text{LaF}_3$  [36] correlate well with the energies of bands observed in the spectra of  $\text{Ln}^{3+}(\text{aq})$ . It comes as no surprise that in a few cases the original assignments must be modified. Moreover, in

addition to the attempt to derive a more self consistent set of intensity parameters for  $\text{Ln}^{3+}$ (aquo) based on an improved understanding of the energy level scheme, it was of interest to use such a set as the basis for comparison with recently determined values of  $\Omega_\lambda$  for  $\text{An}^{3+}$ (aquo) in the heavy half of the 5f-series. Finally, we are presently in a better position than Judd was in 1962 with respect to the evaluation of overlap integrals and energy differences included in the interactions which contribute to the magnitude of  $\Omega_\lambda$ , both for the lanthanides and the actinides; so the results of new model calculations are reported.

## II(B). Intensity Analysis of Lanthanide Solution Spectra

As suggested in the previous discussion, the free-ion energy level calculations for  $\text{Ln}^{3+}:\text{LaF}_3$  provide both a basis for comparison with the original assignments made to absorption bands observed for  $\text{Ln}^{3+}$ (aquo) ions and in some cases require slightly modified values of  $[\mathbf{U}(\lambda)]^2$ . However no large changes in the values of  $\Omega_\lambda$  previously computed were to be expected, and none have been observed. What does emerge is a similar, somewhat more self-consistent, but on the basis of independent confirmation more firmly-based set of  $\Omega_\lambda$ , Table (II-1). Details of the calculations are readily available from other sources [43].

In the new evaluation, we investigated changes in the values of  $\Omega_\lambda$  that could result from changing the nature of the fitting algorithm. Given an equation of the form

$$P/\sigma = \xi = \Omega_2 [\mathbf{U}^{(2)}]^2 + \Omega_4 [\mathbf{U}^{(4)}]^2 + \Omega_6 [\mathbf{U}^{(6)}]^2$$

we originally chose to directly minimize the differences in  $\xi(\text{observed}) - \xi(\text{calculated})$ , using a least-squares fitting procedure to obtain the optimum values of  $\Omega_\lambda$ . This method automatically weights the fit in favor of the transitions with the largest values of  $\xi$ . We have now also examined the values of  $\Omega_\lambda$  arising when the expression minimized was  $\{1 - (\xi(\text{calculated})/\xi(\text{observed}))\}^2$  and it is these values that are given in Table II-1. While there are small differences between the results of the two methods of fitting, no major discrepancies emerge. In several cases individual levels which tend to distort the fit when included in the parametrization can be readily identified. These are almost exclusively cases in which the  $\mathbf{U}^{(2)}$  matrix elements are very large. An important aspect of the parametrization as a whole is the apparent but small average decrease in the magnitude of  $\Omega_\lambda$  over the series. The consistency of the new parameter values tends to emphasize the disproportionately large values of  $\Omega_2$  and  $\Omega_6$  for  $\text{Pr}^{3+}$ , and of  $\Omega_6$  for  $\text{Nd}^{3+}$ . Since the values of the matrix elements of  $\mathbf{U}(\lambda)$  for  $\text{Pr}^{3+}$  and  $\text{Nd}^{3+}$  are consistent with those calculated for other members of the series, the larger

values of  $\Omega_\lambda$  reflect disproportionately intense transitions. A qualitative difference in the intensities of several bands in  $\text{Pr}^{3+}$  and  $\text{Nd}^{3+}$  compared to other members of the series can also be seen in Figs. II-1, II-2.

Several general characteristics of the fit values of  $\Omega_\lambda$  in Table II-1 that were discussed in our first publications on the subject are still evident. The value of  $\Omega_2$  in aqueous solution is generally small and poorly determined. It does not enter in the calculation of  $P$  for many of the levels since for many transitions the value of  $[\mathbb{Y}^{(2)}]^2$  is zero or very small. As a consequence, the intensities of transitions for the  $\text{Ln}^{3+}$  aquo ion spectra are almost entirely reproduced by a two parameter model.

Considerable interest in the Judd-Ofelt theory has been generated by the fact that it readily accommodates and indeed it predicted those transitions which were subsequently designated as hypersensitive [50-52]. This refers to the characteristic band intensity patterns of  $\text{Ln}^{3+}$  ions in some media--crystals, solutions, and vapor complexes, where one or two lanthanide transitions gain significant intensity relative to all of the other transitions and can indeed become extremely intense. One of the striking examples is  $\text{Ho}^{3+}$  in tetrabutylammonium nitrate-nitromethane, compared to  $\text{Ho}^{3+}$  in 1 M  $\text{HNO}_3$ , Fig. II-3 [53]. Hypersensitive transitions correspond to those with large values of  $[\mathbb{Y}^{(2)}]^2$ , and thus can readily be identified from any tabulation of these matrix elements.

Much of the discussion of intensities in recent years has centered on the mechanism of this hypersensitivity, and useful ideas have been generated. However, in view of the extensive literature, the available reviews thereof, and since our interests here are in aqueous solution spectra where it appears that the hypersensitive bands exhibit a minimum of intensity, our attention will focus on the values of the two other parameters,  $\Omega_4$  and  $\Omega_6$ .

#### II(C). Model Calculation of $T_\lambda$

Except for the work of Judd [44] and a subsequent publication by Krupke [54] which dealt with  $\text{Ln}^{3+}:\text{LaF}_3$  and  $\text{Y}_2\text{O}_3$  but utilized most of the same assumptions made by Judd, there appear to have been no attempts to consider the results of more recent Hartree-Fock calculations and systematic evaluations of the energy level schemes of f-elements in reviewing the model calculation of  $\Omega_\lambda$ . In particular no effort has been made to carry out such a calculation for the 5f-series.

Although a recent review of the intensity calculations for  $\text{An}^{3+}(\text{aquo})$  had to characterize them as poorly determined and

incomplete [13], new experimental data have been obtained and on the basis of extensive analyses of  $Bk^{3+}$ (aquo) and  $Cf^{3+}$ (aquo) spectra, it is now possible to discuss intensity relationships over the whole of the series. This type of approach, the comparison of actinide and lanthanide spectra based on model calculations, as well as the comparison of intensities in the lighter and heavier members of each series, is in any case probably more relevant and illuminating, than the question of how accurately the model reproduces the values of  $\Omega_\lambda$  obtained experimentally for a particular ion.

If in Judd's expression, Eq. II-3, we replace  $v(\text{sec}^{-1})$  by  $c\sigma(\text{cm}^{-1})$  and correspondingly in Eq. (II-4) make the substitution which leads to Eq. (II-5), we have

$$\Omega_\lambda = (2\lambda + 1) \sum_t (2t + 1) B_t \Xi^2(t, \lambda) \quad (\text{II-6})$$

where  $t$  is an index which takes values consistent with a 3-j symbol in the expression for  $\Xi(t, \lambda)$ . There are two quantities to be evaluated,  $B_t$  and  $\Xi(t, \lambda)$ .

As noted earlier,  $B_t$  expresses the interaction of the environment with the central ion. In his evaluation of this quantity for  $Ln^{3+}$ (aquo), Judd [44] chose  $GdCl_3 \cdot 6H_2O$  [55] as a structural model and obtained an expression for  $B_t$  as a function of an appropriate water dipole-metal ion separation  $R$ , and a quantity related to the dipole moment of a typical water molecule in the inner coordination sphere,  $\mu$ .

$$B_t = \left[ \frac{\mu e(t+1)}{(2t+1) R^{t+2}} \right]^2 \sum_{i,j} P_t(\cos \omega_{ij}) \quad (\text{II-7})$$

with this expression, assuming a similar geometric arrangement of the dipoles for all  $Ln^{3+}$ ,  $\sum_{i,j} P_t(\cos \omega_{ij})$ , Judd computed values of  $B_t$  for a typical light lanthanide,  $Nd^{3+}$ , and a typical heavy lanthanide,  $Er^{3+}$ , using appropriate values of  $\mu$  and  $R$ .

We could go to the trouble of constructing a different model that would take into account the fact that in the light half of the 4f series the coordination is probably 9-fold, possibly similar to that in  $Nd(Et SO_4)_3 \cdot 9H_2O$  or  $LaCl_3$ , while for the heavy members of the series there is a predominant 8-fold coordination [56] with a possible square antiprismatic structure. However, in attempting to develop a new structural model we would be left with many of the same approximations that Judd found necessary to invoke such as neglect of all but a first coordination sphere and

the treatment of the water molecules as point charges. Judd made allowance for some difference in the value of  $B_t$  as a function of different ionic radius and effective charge, and it is unlikely that this term would represent anything more than a gradual variation over the series even if a "superior" ionic model could be constructed. We have consequently adopted the original mode of calculation. A new set of effective radii,  $R$ , and dipole moments,  $\mu$ , were computed after averaging the nearest neighbor metal- $H_2O$  distances from available data [57].

$$E(t, \lambda) = 2 \sum_t (2\ell+1)(2\ell'+1)(-1)^{\ell+\ell'} \begin{Bmatrix} 1 & \lambda & t \\ \ell & \ell' & \ell \end{Bmatrix} \begin{pmatrix} \ell & 1 & \ell' \\ 0 & 0 & 0 \end{pmatrix} \begin{pmatrix} \ell' & t & \ell \\ 0 & 0 & 0 \end{pmatrix}$$

$$\frac{\langle nl|r|n'\ell'\rangle \langle nl|r^t|n'\ell'\rangle}{\Delta(n'\ell')} \quad (II-8)$$

Since we are only interested in  $f^N$ -configurations and assuming that the  $f^{N-1}d$ -configuration is the excited configuration that most strongly interacts with  $f^N$ , we have:

$$E(t, \lambda) = -70 \sum_t \begin{Bmatrix} 1 & \lambda & t \\ 3 & 2 & 3 \end{Bmatrix} \begin{pmatrix} 3 & 1 & 2 \\ 0 & 0 & 0 \end{pmatrix} \begin{pmatrix} 2 & t & 3 \\ 0 & 0 & 0 \end{pmatrix}$$

$$\frac{(nf|r|n'd)(nf|r^t|n'd)}{\Delta(n'd)} \quad (II-9)$$

We have to evaluate one 6-j and two 3-j symbols expressing the coupling of angular momenta. From the second 3-j symbol in (II-9) we have  $t \leq 5$  and odd, so for  $\Omega_4$  and  $\Omega_6$  only  $t = 3$  or 5 can be involved. Variation in  $E(t, \lambda)$  along the series is clearly a function of the radial integrals,

$$(nf|r^t|n'd) = \int_0^\infty R(nf) r^t R(n'd) dr$$

and of the energy differences between  $f^N$  and  $f^{N-1}d$  electronic states.

Judd [44] used values of radial integrals available at the time. Since then, relativistic Hartree-Fock codes have been used to compute the requisite integrals for both the 4f and 5f-elements. Typical results for  $Ln^{3+}$  are shown in Table II-2. It is apparent that the relativistic values are somewhat smaller than those used originally by Judd. They are also smaller than the expectation values  $\langle r^n \rangle$  computed earlier by Lewis [58]. This further emphasizes the fact that meaningful comparisons between experiment

and theory are primarily to be made in systematic trends and in this case in comparisons between two series, 4f and 5f, using a single consistent method of calculation.

The other quantity to be evaluated in Eq. II-9 is  $\Delta(n'd)$ . In 1971, Brewer [59] published a very important compilation of spectroscopic data that for the most part was not available to Judd in 1962. Some pertinent results are illustrated in Fig. II-4 which shows the energies of the ground states of several excited configurations relative to the  $f^N$ . We could take the results for  $f^{N-1}d$  directly, but they refer to gaseous free-ion spectra and we are concerned with solutions. The appropriate lowering of energy due to the effects of the condensed phase is  $15-20000 \text{ cm}^{-1}$  [60]. It can be seen from Table II-3 that while this does not appreciably change the value of  $\Delta(n'd)$  originally used by Judd for  $\text{Nd}^{3+}$ , the new value for  $\text{Er}^{3+}$  is lower. In considering the role of the lowest-lying  $f^{N-1}d$ -configuration in Eq. II-9, Judd showed that contributions from related configurations of the type  $f^{N-1}n'd$  and  $n'd^9f^{N+1}$  could be neglected while those for the  $f^{N-1}n'g$  could be approximated and thus included in the sum. Overlap with continuum functions was not considered. In the present development we limit consideration to the perturbing effects of lowest excited  $n'd$ -configuration.

The new results for  $\Omega_1$ , Table II-4, do not differ importantly from those computed by Judd, whose values corresponding to  $\Omega_4$  and  $\Omega_6$  were a close enough approximation to experiment to make it possible to argue that small adjustments in the magnitude of the interactions considered would reasonably account for the difference and no additional mechanisms for enhancement of the model-computed intensity needed be invoked. We have already commented on the fact that the radial integrals quoted here are considerably smaller than those used by Judd. What does become apparent from the form of Eq. II-8 and the results shown in Table II-2 and Fig. II-4, is that the values of  $\Omega_4$  and  $\Omega_6$  are predicted to follow a pattern in which there is a decrease in magnitude from  $f^2$  to  $f^7$ , an increase from  $f^7$  to  $f^8$  and a second pattern of decrease from  $f^8$  through  $f^{12}$ . The values of the fit parameters given in Table II-4 are consistent with the prediction for the heavy lanthanides, but the pattern is less well established for the light members of the series. However, it is apparent that the experimentally established parameter values for  $\text{Gd}^{3+}(\text{aquo})$  do not follow the expected pattern. The disproportionately large values for  $\Omega_2$  and  $\Omega_6$  in  $\text{Pr}^{3+}$ , and for  $\Omega_6$  in  $\text{Nd}^{3+}$  reflect more intense transitions than revealed in other comparable members of the series.

### II(D). Intensity Analysis of Actinide Solution Spectra

In developing the basis for comparing intensities of transitions characteristic of  $An^{3+}$ (aquo) and  $Ln^{3+}$ (aquo), it is important to be aware of the relative density of states for the  $4f^N$  and  $5f^N$ -configurations as indicated for the light half of the two series in Fig. II-5. It is apparent that the  $f^N$ -states occur within a smaller energy range in the actinides. As a consequence, particularly in  $U^{3+}$ ,  $Np^{3+}$ , and  $Pu^{3+}$ , the population density over the optical range of prime interest here is large. It is difficult to make very many meaningful assignments to  $An^{3+}$ (aquo) even though the corresponding states have been well characterized in crystals [13]. In addition to the higher density of states in the light actinides, the intensities of individual  $An^{3+}$ (aquo) transitions can be as much as a factor of 10-100 greater than for corresponding lanthanides. As indicated in Fig. II-6, the average intensity of a transition decreases significantly with increasing  $Z$ . It reaches a minimum near  $Cm^{3+}$  and remains essentially constant over the heavy half of the series, Fig. II-7.

While an intensity analysis of  $Cm^{3+}$ (aquo), the analog of  $Gd^{3+}$ (aquo), was published earlier [61], and intensity-related arguments were used to aid the interpretation of the energy level structure in  $Es^{3+}$ (aquo) [62], it is only very recently that new experimental work has made possible a detailed interpretation of the spectra of  $Bk^{3+}$ (aquo) and  $Cf^{3+}$ (aquo).

The Judd intensity parameters for the heavier actinides are set out in Table II-5. The individually determined parameters for  $Cm^{3+}$ ,  $Bk^{3+}$ , and  $Cf^{3+}$  were extrapolated to give a set for  $Es^{3+}$  which was not only found to be consistent with earlier work but actually gave an improved correlation with the observed spectrum. The absorption spectrum for  $Es^{3+}$ (aquo) shown in Fig. II-7 is a composite of a number of measurements made using micro absorption cells. The increasing background upon which the spectrum is superimposed is due to light scattering and radiolysis products.

The intensity parameters derived from fitting the experimental data for  $Bk^{3+}$ (aquo) and  $Cf^{3+}$ (aquo) could be interpreted in detail by the Judd theory, as indicated in Table II-6 for  $Bk^{3+}$ . The highly forbidden character of the spectrum in the lanthanide analog,  $Tb^{3+}$ (aquo), which is manifest in weak absorption bands and smaller than average values for  $[U(\lambda)]^2$ , is not evidenced in  $Bk^{3+}$ (aquo) where intensities and matrix element magnitudes are average for the heavy actinides. This difference in character can be traced to the increased spin-orbit coupling which results in a greater mixing of states in  $Bk^{3+}$  as indicated in the ground term eigenvector which is 95.6%  $^7F$  in  $Tb^{3+}$  and only 72.2%  $^7F$  in  $Bk^{3+}$ . The first  $f \rightarrow d$  transitions in  $Tb^{3+}$  and  $Bk^{3+}$  both occur in

the near ultraviolet range with the spin-forbidden  $^9D$  ( $f^8 \rightarrow f^7d$ ) state in  $Tb^{3+}$  centered near  $38000\text{ cm}^{-1}$  and that in  $Bk^{3+}$  near  $34000\text{ cm}^{-1}$ , Fig. II-8. As was the case for this band in  $Tb^{3+}$  [48], the superimposed structure in  $Bk^{3+}$  can be analyzed in terms of  $f \rightarrow f$  transitions.

Comparison of the intensity parameters for analog members of the lanthanide and actinide series in Tables II-1 and II-5 shows a factor of 5-10 increase in intensity in the heavy actinides compared to the lanthanides. At this point it is evident that Judd's formalism is fully applicable to the experimentally observed intensity patterns observed for 5f as well as 4f-elements so that it remains to explore the correlation with the model calculations of  $\Omega_\lambda$ --again restricted to  $\Omega_4$  and  $\Omega_6$ .

In approaching the model calculation of  $\Omega_4$  and  $\Omega_6$  for  $An^{3+}(\text{aquo})$ , we consider first the analog of Eq. II-7. The problem is simplified because of the close relationship between the ionic radii characteristic of the trivalent ions in the two series. As an approximation the radii of  $Ln^{3+}(f^N)$  and  $An^{3+}(f^{N+2})$  are usually quite comparable. Thus for example for the  $MCl_3 \cdot 6H_2O$  structure in the lanthanides  $M \leftrightarrow (2)H_2O$  distances range from  $2.449\text{ \AA}$  in  $M=Nd$  to  $2.312\text{ \AA}$  in  $M=Lu$  [57] while for  $M=Am$  the distance is  $2.440\text{ \AA}$  [63]. We consequently do not expect any significant change in the contribution of  $B_t$ , Eq. III-7, computed for a characteristic light (or for a heavy) lanthanide ion or actinide ion, and the method of approximation used by Judd appears to be equally applicable to the two series.

One of the interesting questions that arises is whether there is a change in inner sphere hydration number in the  $An^{3+}(\text{aquo})$  series corresponding to that deduced for the lanthanides. Recent electromigration studies suggest that such a change could be occurring in the region of  $Cf^{3+}$  -  $Es^{3+}$  [56]. However neither the absorption spectra of  $Ln^{3+}(\text{aquo})$ , nor that of  $An^{3+}(\text{aquo})$  appear to provide an indication of this change. The hypersensitive transitions in both the 4f and 5f-series, normally the most sensitive spectroscopic monitors of a changing ionic environment, uniformly show a minimum of intensity in the aquo ions. Thus aquo ion spectra serve as a standard for judging increased intensity in other environments, without providing any internal evidence for structural modification. However, in the role of providing a standard for judging increased intensity, comparisons to spectra in crystal matrices can indicate where in a series structural changes appear to be occurring.

If we compare the spectrum of  $Cf^{3+}(\text{aquo})$ , Fig. (II-7), and that of  $CfCl_3$  (hexagonal  $LaCl_3$ -type structure) [64], there is a similar energy and band intensity pattern with the exception of

the increased intensity in the hypersensitive transition in CfCl<sub>3</sub> near 11400 cm<sup>-1</sup>. Thus, if the structure is correctly identified, we have a case of what would appear to be a small distortion giving rise to an enhancement in intensity, a unique case for the LaCl<sub>3</sub>-type structure. On the other hand, if there is a distortion toward the AlCl<sub>3</sub>(YC<sub>13</sub>)-phase which is characteristic of the heavy lanthanide chlorides [65] then having examined other cases we would expect that there would be increased intensity in the indicated hypersensitive transition. In our absorption spectra study of thin films of CfCl<sub>3</sub> [66] we identified the sample by X-ray analysis as exhibiting the hexagonal LaCl<sub>3</sub>-type structure. While there was no apparent increased intensity near 11400 cm<sup>-1</sup> relative to Cf<sup>3+</sup>(aquo), the 298 K spectra of the thin film were admittedly broad and diffuse and thus not definitive in this respect. What can be said is that there is some evidence of distortion suggesting a tendency toward structural change at this point in the An<sup>3+</sup> series.

For a related case, Es<sup>3+</sup>(aquo) compared to Es<sup>3+</sup>:LaCl<sub>3</sub> [67], the correlation between the two spectra is very good both in terms of energy and band intensity including the hypersensitive transition. This conforms to similar behavior for the lanthanides in this matrix. On the contrary there is evidence of increased intensity in the hypersensitive band in EsF<sub>3</sub> near 20000 cm<sup>-1</sup> [68], a sample for which an X-ray diffraction pattern could not be obtained. Alternative structures [65] are the LaF<sub>3</sub>-type (not conducive to increased intensity in hypersensitive transitions) and the YF<sub>3</sub>-type which is known to induce increased intensity in the hypersensitive transitions. Since the results are consistent with a change in crystal structure from the LaF<sub>3</sub>-type typical of preceding members of the series, a change in hydration number occurring at this point in the series would not be unexpected.

Returning to the calculation of  $\Omega_\lambda$ , in addition to the B<sub>t</sub> term, Eq. II-7, the overlap integrals and energy differences indicated in Eq. II-9 must be computed. We limit consideration, as was done for the lanthanides, to overlap with the n'd configuration. Consequently the 6-j and 3-j symbols of Eq. II-8 are identical for the 4f- and 5f-series. The overlap integrals computed using a relativistic HF code and analogous to those for the lanthanides (Table II-2) are set out in Table II-7.

The f<sup>N</sup>  $\rightarrow$  f<sup>N-1</sup>d transitions in the actinides occur at somewhat lower energies than for the corresponding lanthanides as noted earlier and the hydration energy correction relative to the gaseous free-ion data is apparently less in the light than in the heavy portion of the 5f-series. The estimated values of  $\Delta(n'd)$  are given in Table II-8. The appearance of intense absorption bands in the visible to ultraviolet range of the spectra of many

of the  $An^{3+}$ (aquo) ions Fig. II-3, II-4, provides a much better basis for a consistent assignment of an energy for the first  $f \rightarrow d$  transition than is the case for  $Ln^{3+}$ (aquo) where few such transitions lie low enough in energy to be observed.

In comparing the intensity parameters for  $An^{3+}$ (aquo) determined by fitting the experimental data and those based on a model calculation, Table II-9, it is at once apparent that the agreement is similar to that found for the lanthanides. Thus the very intense transitions in the light actinides are well correlated with the close proximity of, and the increased overlap with the  $n'd$  configurations. The model computed intensity decreases markedly with  $Z$  except for the break at  $f^7$  corresponding to a sudden change in  $\Delta(n'd)$ , while this trend is less pronounced in the heavy members of both the 4f and 5f series. Since we have considered only the effects of the  $(n'd)$  configurations, inclusion of the effects of other opposite parity interactions should be investigated. Judd's estimates of the effects of the  $n'g$ -configurations did show a greater contribution to the heavy members of the  $Ln^{3+}$ (aquo) series [44] and this was also emphasized by Krupke [54].

A comparison of the model computed intensity parameter values for  $Ln^{3+}$ (aquo) and  $An^{3+}$ (aquo), Tables II-4 and II-9, further shows that the magnitude of the increased intensity between the two series is correctly predicted, and thus can reasonably be correlated with the larger values computed for the radial overlap integrals. The similarity in the values for other  $Ln^{3+}$ (aquo) and  $An^{3+}$ (aquo) dependent quantities included in the model makes identification of the role of the overlap integrals particularly clear in this case.

Not all of the observed intensity patterns are satisfactorily accounted for in the model. The fact that the fit parameters for  $f^7$  are larger than those for  $f^8$  in both the 4f- and 5f-series is not explained. The role of J-mixing as a possible explanation for the observation of nominally forbidden transitions, particularly  $^7F_0 \rightarrow$  odd  $J$  transitions in the  $f^6$ -configurations needs to be explored, as do similar perturbing effects in  $Bk^{3+}$ . However it is clear that Judd's development of the intensity analysis continues to give us very important insights into the physics of these unique f-elements.

### III. FLUORESCENCE STUDIES OF THE TRIVALENT LANTHANIDE AND ACTINIDE AQUO IONS

One of the important features of a successful analysis of the intensities of the f-elements in solution is that it provides the basis for calculating the radiative lifetime characteristic

of any given excited state [43]. Most excited states are primarily relaxed by non-radiative mechanisms, but for those that exhibit a measurable fluorescence it is useful to point out the relationship:

$$(\tau_T)^{-1} = A_T(\psi J) + W_T(\psi J) \quad (\text{III-1})$$

where  $\tau_T$  is the observed lifetime of a particular excited state,  $A_T(\psi J)$  is the total radiative relaxation rate and  $W_T(\psi J)$  is the total non-radiative relaxation rate. The rate of relaxation computed from the intensity analysis corresponds to the case in which  $W_T=0$ . Thus there is a limited range of relative rates of  $A_T$  and  $W_T$  in which both contribute importantly, and where consequently, the difference  $(\tau_T)^{-1} - A_T(\psi J) = W_T(\psi J)$  can provide an independent method of assessing  $W_T$ . This can be very useful information when exploring the mechanisms of non-radiative relaxation.

Another instructive use of  $A_T(\psi J)$  is in the prediction of pathways of radiative relaxation. A given excited state is coupled to each state that is lower in energy. Knowledge of which states are most strongly coupled to the excited state leads to the prediction of the energies of strong fluorescing lines. Of course if the predominant mechanism of relaxation involves non-radiative processes, no fluorescence will be observed.

The general form of the probability for spontaneous relaxation of an excited state [69], is

$$A(\psi J, \psi' J') = \frac{64\pi^4 \sigma^3}{3h} (\psi J | D | \psi' J')^2 \quad (\text{III-2})$$

where  $\psi J$  and  $\psi' J'$  are the initial and final states,  $A$  is the spontaneous transition probability per unit time,  $\sigma(\text{cm}^{-1})$  the energy gap between the states, and  $D$  is the dipole operator which we can replace by the electric and magnetic dipole line strengths. Following Axe [49], Eq. III-1 can be written

$$A(\psi J, \psi' J') = \frac{64\pi^4 \sigma^3}{3h (2J+1)} \left[ X' \bar{F}^2 + n^3 \bar{M}^2 \right] \quad (\text{III-3})$$

where  $J$  in this case refers to the initial excited state, *not* the ground state, and  $X' = n(n^2 + 2)^2/9$ . The electric dipole ( $\bar{F}^2$ ) and magnetic dipole ( $\bar{M}^2$ ) operators are those defined previously in terms of static absorption intensities, so the required matrix elements for transitions of interest can be readily computed.

$$\bar{F}^2 = e^2 \sum_{\lambda=2,4,6} \Omega_{\lambda} (\psi J || U^{(\lambda)} || \psi' J')^2 \quad (III-4)$$

$$\bar{M}^2 = e^2 (\psi J || L + 2S || \psi' J')^2 / 4m^2 c^2 \quad (III-5)$$

Further details of the computation are given in [43].

Calculation of spontaneous emission rates and the lifetimes are summarized by Eq. III-1, and by the expression:

$$A_T(\psi J) = \sum_i (\psi J, \psi' J')_i \quad (III-6)$$

where the sum runs over all states with energy less than that of  $\psi J$ . Thus in absorption a particular state can be populated. In emission, relaxation to all lower-lying states is summed over to give a total rate. The branching ratio,  $\beta_R$ , from the relaxing state to a particular final state is given by

$$\beta_R (\psi J, \psi' J') = \frac{A(\psi J, \psi' J')}{A_T(\psi J)} \quad (III-7)$$

The principal fluorescing states of the lanthanide aquo ions were known long before their lifetimes could be accurately measured. Thus, based on work completed in the 1930's, Fig. III-1, the excited states of interest to the type of analysis developed here are well characterized. Selected values of the measured radiative lifetimes of some of the excited states of  $\text{Ln}^{3+}$ (aquo) are compared with those computed from spontaneous radiative relaxation rates in Table III-1. It is apparent that even for  $\text{Gd}^{3+}$ (aquo), non-radiative relaxation is of major importance since based on Eq. III-1, assuming  $\tau_{\text{H}_2\text{O}} = 2 \text{ msec}$ , and computing  $A_T(^6\text{P}_{7/2}) = 92 \text{ sec}^{-1}$ , we see that  $W_T(^6\text{P}_{7/2}) = 408 \text{ sec}^{-1}$ .

### III(A). Branching Ratio Calculations

While the experimental observation of fluorescence of lanthanide ions in aqueous solution predated our ability to predict the patterns of excited state relaxation, it is still useful to point out some of the features of the calculation of branching ratios. Fig. III-2 illustrates the fact that a fluorescing excited state, in this case  $^5\text{D}_4$  of  $\text{Tb}^{3+}$ , may be particularly strongly coupled to one or two of the lower-lying states, and not necessarily to the ground state. Of course the  $\sigma^3$  dependence in Eq. III-3

will strongly select a large energy gap. For  $Tb^{3+}$ (aquo), the  $^5D_4$  state is most strongly coupled to the (excited)  $^7F_5$  state. Consequently the prediction would have been that the strongest band in fluorescence originating from the  $^5D_4$ -state would be found at  $20450-2100 = \sim 18350 \text{ cm}^{-1}$ ; which of course is consistent with experimental results [70]. The branching ratios calculated for  $Tb(NO_3)_3$  in a molten  $LiNO_3-KNO_3$  eutectic solution at  $\sim 150^\circ$  are included in Fig. III-2 for comparison [71]. It was pointed out earlier that of the three parameters,  $\Omega_\lambda$ ,  $\Omega_2$  is most sensitive to changes in the ionic environment. In the molten nitrate salt spectrum of  $Tb^{3+}$  a relative increase in the intensity of  $U^{(2)}$ -dependent transitions is reflected in a large value for  $\Omega_2$ . Both  $\Omega_4$  and  $\Omega_6$  also differ somewhat from the  $Tb^{3+}$ (aquo) values. However, the calculated branching ratios even more strongly select the  $^5D_4 \rightarrow ^5F_5$  transition. The principal lasing frequency associated with fluorescing excited states of the lanthanides can usually be predicted from branching ratio calculations.

Absorption and excited state relaxation are processes that are in equilibrium; consequently, it is possible to use properly corrected oscillator strengths obtained from the analysis of fluorescence spectra as input to the calculation of  $\Omega_\lambda$  along with oscillator strengths computed in the usual analysis of absorption spectra. Although recorded in the gas phase, not in solution, the  $TbCl_3-AlCl_3$  gas-phase complex is an example of a system in which both absorption and fluorescence spectra were utilized in computing  $\Omega_\lambda$  [72]. The measured fluorescence spectrum shown in Fig. III-3 includes bands from several different parent states, but the relative intensities of those transitions attributed to  $^5D_4 \rightarrow ^7F_5$  and  $^5D_4 \rightarrow ^7F_6$  are consistent with the intensity patterns expected based on the branching ratios.

Recently the first fluorescence study of an  $An^{3+}$  ion in aqueous solution was carried out [73]. We have now begun a systematic investigation of  $An^{3+}$ (aquo) fluorescence [74] and it is as part of this study that branching ratio calculations are aiding the interpretation of new experimental data. The results of the intensity analyses for the  $Cm^{3+}$ ,  $Bk^{3+}$ ,  $Cf^{3+}$ , and  $Es^{3+}$  aquo ions cited previously have been used to compute the branching ratios indicated in Fig. III-4.

For  $Cm^{3+}$ (aquo), the actinide analog of  $Gd^{3+}$ , the most important fluorescing state is the first excited  $^6P_{7/2}$ -state. Selective laser excitation in  $D_2O$  yielded a measured lifetime of 940  $\mu\text{sec}$  [73] compared to a computed purely radiative lifetime of 1.3 msec. Excitation at  $25445 \text{ cm}^{-1}$  was found to be relaxed non-radiatively to the  $^6P_{7/2}$  state, the only state from which fluorescence was observed. Similarly, excitation of  $Bk^{3+}$ (aquo) at  $25575 \text{ cm}^{-1}$  resulted in fluorescence being observed only from the  $J=6$

state near  $16000\text{ cm}^{-1}$ . In the latter case the results are consistent with the indicated branching ratio. No intermediate level is more strongly coupled to the fluorescing state than the ground state is. However, because of the relatively narrow energy gap between the fluorescing state and the next lower-energy state, the fluorescence lifetime is very short. The dependence of lifetime on energy gap is discussed in a subsequent section.

Branching ratio calculations for the most probable fluorescing transitions of  $\text{Cf}^{3+}(\text{aquo})$  are shown in Fig. III-4. Fluorescence from both of these  $\text{Cf}^{3+}(\text{aquo})$  transitions is predicted to be quite weak with lifetimes much less than 0.1 microseconds expected since the energy gaps are even narrower than in the fluorescing transition of  $\text{Bk}^{3+}(\text{aquo})$ . We exclude the  $11/2$  state at about  $6500\text{ cm}^{-1}$  from consideration since nanosecond response photodetectors for this spectral region are quite insensitive compared to photomultipliers. Selective laser excitation of  $\text{Es}^{3+}(\text{aquo})$  at  $20070\text{ cm}^{-1}$  gives rise to detectable fluorescence from the  $J=5$  state at about  $9500\text{ cm}^{-1}$  (Fig. III-4). In detecting fluorescence characteristic of  $\text{Es}^{3+}(\text{aquo})$ , it should be noted that we are dealing with an intensely  $\alpha$ -active isotope ( $t_{1/2} = 21.5$  days). Use of current laser and photodetection technology has enabled us to measure the fluorescence lifetime of  $\text{Es}^{3+}(\text{aquo})$  in  $\text{D}_2\text{O}$  solution at concentrations as low as  $5 \times 10^{-6}$  molar.

We have not addressed the calculation of branching ratios for the light members of the  $3+$  aquo actinide ion series. The high density of  $5f$  states in the energy level structures of these ions makes it improbable, with the possible exception of  $\text{Am}^{3+}$ , that measurable fluorescence will be found even in  $\text{D}_2\text{O}$  solution using the techniques at hand [73, 74].

### III(B). Non-Radiative Relaxation

In crystalline hosts, it has been shown that the quantitative treatment of non-radiative relaxation mechanisms is extremely complex. Multiphonon orbit-lattice relaxation has been recognized as an important mode of decay, and experimentally the dependence of fluorescence quenching on the energy gap ( $\Delta E$ ) between the fluorescing state and the next lower-energy state, has been well established.

Investigations of the temperature dependence of the multiphonon relaxation rates have shown that the decay usually involves emission of high-energy optical phonons. In  $\text{LaCl}_3$ , for example, the phonon density of states cuts off at  $\sim 260\text{ cm}^{-1}$ . It was found that for crystals the process was adequately represented by,

$$W = \beta e^{\alpha \Delta E}$$

(III-8)

where  $\beta$  and  $\alpha$  are parameters characteristic of the particular lattice. The energy gap,  $\Delta E$ , thus determines the number of high energy phonons that must be emitted simultaneously to absorb the requisite energy. The multiphonon process becomes less probable as the number of phonons that must be simultaneously excited to conserve energy increases. Recalling the rule of  $\sim 1000 \text{ cm}^{-1}$ , which corresponds to a minimum  $\Delta E$  required before fluorescence would be expected in  $\text{LaCl}_3$  host, it is clear that the emission of less than 4-phonons is a process that efficiently competes with the radiative relaxation modes.

Experiments exploring non-radiative modes of relaxation in solution actually paralleled work in the solid state in the early 1960's. In a particularly enlightening series of papers Kropp and Windsor [75] examined the effects that the substitution of  $\text{D}_2\text{O}$  for  $\text{H}_2\text{O}$  had on the fluorescent lifetimes of a number of different states in rare earth ion spectra. These results illustrate the sensitivity of the lifetimes to changes in the ionic environment when for all practical purposes no change is observed in the energy or intensity of the absorption bands, i.e., in  $\text{D}_2\text{O}$  and  $\text{H}_2\text{O}$ .

In their pioneering work Kropp and Windsor pointed out that the ratio of the intensity of fluorescence of a given  $\text{Ln}^{3+}$  state in  $\text{D}_2\text{O}$  to that of the same state in  $\text{H}_2\text{O}$  was inversely proportional to the energy gap,  $\Delta E$ . Subsequently, they concluded that the quenching of fluorescence in aqueous solution occurred via  $\text{OH}$  coupled modes and the rate was proportional to the number of such modes associated with the lanthanide ions. Gallagher [76] reached the same conclusion showing that the introduction of a single  $\text{OH}^-$  group into the inner coordination sphere in  $\text{Eu}^{3+}$  was sufficient to reduce the fluorescence lifetime of the  $^5\text{D}_0$  state from 3.9 (pure  $\text{D}_2\text{O}$ ) to 0.12 msec.

This led to the interpretation of the quenching of fluorescence in  $\text{H}_2\text{O}$  ( $\text{D}_2\text{O}$ ) in terms of a multiphonon mechanism involving the transfer of energy to a single vibration mode ( $\text{OH}$ ) excited to high vibrational states. This parallels the interpretation in crystals. The number of phonons required to bridge the gaps characteristic of fluorescing states in  $\text{Ln}^{3+}(\text{aquo})$  using  $\nu_1(\text{OH}) = 3405 \text{ cm}^{-1}$  and  $\nu(\text{OD}) = 2520 \text{ cm}^{-1}$ , are:

	$\Delta E/\nu_1$	
	<u>OH</u>	<u>OD</u>
Gd <sup>3+</sup>	10	13
Tb <sup>3+</sup>	5	6
Eu <sup>3+</sup>	4	5
Dy <sup>3+</sup>	3	4
Sm <sup>3+</sup>	3	4
Nd <sup>3+</sup>	1	2

The lifetimes observed in aqueous solution follow a somewhat similar pattern to that observed in crystals: the higher the order the quenching process (i.e. the larger the number of phonons needed to bridge the energy gap), the lower the non-radiative decay rate  $W_T$ . In Fig. III-5, the logarithm of the non-radiative decay rate constant has been plotted versus the energy gap for the emitting  $\text{Ln}^{3+}(\text{aquo})$  state in  $\text{H}_2\text{O}$  and  $\text{D}_2\text{O}$  solution, using Eq. III-1 and the data in Table III-1. By analogy with doped single crystal studies of lanthanide ion non-radiative decay, a linear relationship might have been expected (see Eq. III-8), but, as is evident from Fig. III-5, only rough linearity is found. As noted by Stein and Wurzberg [77], non-radiative decay of lanthanide ions in solution is most appropriately considered in the "large molecule" limit where the lanthanide ion and its solvation sphere are treated as a single quantum mechanical system. Detailed development of such a theory remains a considerable challenge.

Non-radiative relaxation of aquo lanthanide and actinide ions in solution is even more complex than is the case in doped single crystal studies of these same ions. The greater complexity arises from the wide energy range spanned by the normal vibrational mode frequencies of water and the lack of long range order which is characteristic of liquids. Even inner coordination sphere water molecules exchange on a time scale short compared to the lifetimes of large energy gap fluorescing f states [78]. Initial efforts have been made to understand f electron non-radiative decay in solution, but this is an area in which there is significant potential for development. The Judd-Ofelt theory provides a good approximation to the radiative portion of the experimentally observed lifetimes of 3+ aquo lanthanide and actinide ion fluorescing f electron states, but it is evident that several mechanisms in addition to multiphonon-like processes must be explored to adequately represent the observed non-radiative relaxation rates.

### Acknowledgment

Work performed under the auspices of the Office of Basic Energy Sciences, Division of Nuclear Sciences, U. S. Department of Energy under contract number W-31-109-ENG-38.

### References

1. B. G. Wybourne, Spectroscopic Properties of Rare Earths, John Wiley, New York, 1965.
2. G. H. Dieke, Spectra and Energy Levels of Rare Earth Ions in Crystals, Ed. H. M. Crosswhite and H. Crosswhite, John Wiley, New York, 1968.
3. S. Hüfner, Optical Spectra of Transparent Rare Earth Compounds, Academic Press, New York, 1978.
4. C. A. Morrison and R. P. Leavitt, Handbook of the Physics and Chemistry of Rare Earths, Ed. K. A. Gschneider and L. Eyring, North-Holland Publishing Co., New York, 1982, Vol. 5.
5. C. F. Fischer, The Hartree-Fock Method for Atoms, Wiley-Interscience, New York, 1977.
6. W. T. Carnall, H. M. Crosswhite, R. G. Pappalardo, D. Cohen, S. Fried, P. Lucas, F. Wagner Jr., *J. Chem. Phys.* 61, 4993 (1974).
7. W. T. Carnall, H. Crosswhite, H. M. Crosswhite, J. P. Hessler, N. Edelstein, J. G. Conway, G. V. Shalimoff, R. Sarup, *J. Chem. Phys.* 72, 5089 (1980).
8. F. H. Spedding, *Phys. Rev.* 58, 255 (1940).
9. W. T. Carnall in Section Lectures of the 13th International Conference on Coordination Chemistry, Ed. B. J. Trzebiatowska and M. Rudolf, Polish Academy of Sciences, Warsaw, 1974.
10. K. Rajnak and B. G. Wybourne, *Phys. Rev.* 132, 280 (1965).
11. J. C. Morrison and K. Rajnak, *Phys. Rev.* A4, 536 (1971).
12. H. M. Crosswhite, Colloques Internationaux du C. N. R. S., Spectroscopie des Elements de Transition et des Elements Lourds dans les Solides, 28 Juin - 3 Juillet 1976, Fitions due C. N. R. S., Paris, 1977, p. 65.
13. Jan P. Hessler and W. T. Carnall, ACS Symposium Series No. 131, 349 (1980).
14. J. C. Morrison, *Phys. Rev.* A6, 643 (1972).
15. B. R. Judd, *Phys. Rev.* 141, 4 (1966).
16. H. Crosswhite, H. M. Crosswhite, and B. R. Judd, *Phys. Rev.* 174, 89 (1968).
17. G. Balasubramanian, M. M. Islam, and D. J. Newman, *J. Phys.* B8, 2601 (1975).
18. B. R. Judd, H. M. Crosswhite, and H. Crosswhite, *Phys. Rev.* 169, 130 (1968).
19. H. M. Crosswhite, H. Crosswhite, F. W. Kaseta, and R. Sarup, *J. Chem. Phys.* 64, 1981 (1976).

20. R. D. Cowan and D. C. Griffin, *J. Opt. Soc. Am.* 66, 1010 (1976).
21. H. M. Crosswhite and H. Crosswhite, *Private Communication*.
22. B. R. Judd, *J. Lumin.* 18/19, 604 (1979).
23. B. R. Judd, *Phys. Rev. C13*, 2695 (1980).
24. M. T. Hutchings and D. K. Ray, *Proc. Phys. Soc.* 81, 663 (1980).
25. M. Faucher, J. Dexpert-Ghys, and P. Caro, *Phys. Rev. B21*, 3689 (1980).
26. D. J. Newman, *Adv. Phys.* 20, 197 (1971).
27. D. J. Newman, *J. Phys. C10*, 4753 (1977).
28. D. J. Newman, *Aust. J. Phys.* 31, 489 (1978).
29. H. M. Crosswhite, H. Crosswhite, W. T. Carnall, A. P. Paszek, *J. Chem. Phys.* 72, 5103 (1980).
30. Y. M. Poon and D. J. Newman, *J. Chem. Phys.* 75, 3646 (1981).
31. A. K. Cheetham, B. E. F. Fender, H. Fuess, A. F. Wright, *Acta Cryst. B32*, 94 (1976).
32. A. Zalkin, D. H. Templeton, and T. E. Hopkins, *Inorg. Chem.* 5, 1466 (1966).
33. W. H. Zachariasen, *J. Chem. Phys.* 16, 254 (1948).
34. D. E. Onopko, *Optics and Spectro. Suppl. 4*, USSR Academy of Sciences, 1968; *Optics and Spectro.* 24, 301 (1968).
35. D. J. Newman and M. M. Curtis, *J. Phys. Chem. Solids* 30, 2731 (1969).
36. W. T. Carnall, H. Crosswhite, H. M. Crosswhite, *Energy Level Structure and Transition Probabilities of the Trivalent Lanthanides in LaF<sub>3</sub>*, Argonne National Laboratory Report (1977).
37. C. A. Morrison and R. P. Leavitt, *J. Chem. Phys.* 71, 2366 (1979).
38. P. Caro, J. Derouet, L. Beaury, G. Teste de Sagey, J. P. Chaminade, J. Aride, M. Pouchard, *J. Chem. Phys.* 74, 2698 (1981).
39. H. H. Caspers, H. E. Rast, and J. L. Fry, *J. Chem. Phys.* 53, 3208 (1970).
40. R. P. Leavitt and C. A. Morrison, *J. Chem. Phys.* 73, 749 (1980).
41. L. J. F. Broer, C. J. Gorter, and J. Hoogschagen, *Physica* 11, 231 (1945).
42. J. H. Van Vleck, *J. Phys. Chem.* 41, 67 (1937).
43. W. T. Carnall, Handbook on the Physics and Chemistry of Rare Earths, Ed. K. A. Gschneidner Jr. and L. Eyring, North-Holland, New York, 1979, Vol. 3, p. 171.
44. B. R. Judd, *Phys. Rev.* 127, 750 (1962).
45. G. S. Ofelt, *J. Chem. Phys.* 37, 511 (1962).
46. R. Reisfeld and C. J. Jørgensen, Lasers and Excited States of Rare Earths, Springer, New York, 1977.
47. M. J. Weber, Handbook on the Physics and Chemistry of Rare Earths, Ed. K. A. Gschneidner Jr. and L. Eyring, North-Holland, New York, 1979, Vol. 4, p. 275.
48. J. D. Axe, *J. Chem. Phys.* 39, 1154 (1963).

49. W. T. Carnall, P. R. Fields, and K. Rajnak, *J. Chem. Phys.* 49, 4224, 4443, 4447, 4450 (1968).
50. R. D. Peacock, *Struct. Bonding* 22, 83 (1975).
51. B. R. Judd, *J. Chem. Phys.* 70, 4830 (1979).
52. S. F. Mason, *Struct. Bonding* 39, 43 (1980).
53. W. J. Maeck, M. E. Kussy, and J. E. Rein, *Anal. Chem.* 37, 103 (1965).
54. W. F. Krupke, *Phys. Rev.* 145, 325 (1966).
55. M. Marezio, H. A. Plettinger and W. H. Zachariasen, *Acta Cryst.* 14, 234 (1961).
56. R. Lundquist, E. K. Hulet, and P. A. Baisden, *Acta Chem. Scand.* A35, 653 (1981).
57. *Gmelin Handbuch der Anorganischen Chemie*, 8th Ed., Rare Earth Elements, Part C4a, Springer Verlag, Heidelberg, 1982, p. 185-194.
58. W. B. Lewis, Los Alamos Scientific Laboratory Report LA-DC-11574 (1970).
59. L. Brewer, *J. Opt. Soc. Am.* 61, 1101, 1666 (1971).
60. E. Loh, *Phys. Rev.* 147, 332 (1966).
61. W. T. Carnall and K. Rajnak, *J. Chem. Phys.* 63, 3510 (1975).
62. W. T. Carnall, D. Cohen, P. R. Fields, R. K. Sjoblom, and R. F. Barnes, *J. Chem. Phys.* 59, 1785 (1973).
63. J. H. Burns and J. P. Peterson, *Inorg. Chem.* 10, 147 (1971).
64. J. R. Peterson, R. L. Fellows, J. P. Young, and R. G. Haire, *Radiochem. Radioanal. Ltrs.* 31, 277 (1977).
65. D. Brown, *Halides of the Lanthanides and Actinides*, J. Wiley, New York, 1968.
66. W. T. Carnall, S. Fried and F. Wagner, Jr., *J. Chem. Phys.* 58, 1938 (1973).
67. R. L. Fellows, J. R. Peterson, J. P. Young and R. G. Haire, *The Rare Earths in Modern Science and Technology* (G. J. McCarthy and J. J. Rhyne, Ed.) Plenum Press, New York, 1978, p. 493.
68. D. D. Ensor, J. R. Peterson, R. G. Haire, and J. P. Young, *J. Inorg. Nucl. Chem.* 43, 2425 (1981).
69. E. U. Condon and G. H. Shortley, *The Theory of Atomic Spectra*, Cambridge University Press, London, 1957, pp. 91-109.
70. W. R. Dawson, J. L. Kropp, and M. W. Windsor, *J. Chem. Phys.* 45, 2410 (1966).
71. W. T. Carnall, J. P. Hessler, and F. Wagner, Jr., *J. Phys. Chem.* 82, 252 (1978).
72. J. A. Caird, W. T. Carnall, J. P. Hessler, *J. Chem. Phys.* 74, 3225 (1981).
73. J. V. Beitz and J. P. Hessler, *Nucl. Tech.* 51, 169 (1980).
74. J. V. Beitz, W. T. Carnall, D. W. Wester and C. W. Williams, Lawrence Berkeley Laboratory Report LBL-12441, 1981.
75. For a review of some of the relevant work of Kropp and Windsor see Reference 43.

76. P. K. Gallagher, J. Chem. Phys. 43, 1742 (1965).
77. G. Stein and E. Würzberg, J. Chem. Phys. 62, 208 (1975).
78. J. Burgess, Metal Ions in Solution, John Wiley, Sussex, 1978, p. 317.
79. J. V. Beitz, Unpublished Results, Argonne National Laboratory, 1982.

TABLE I-1.

ELEMENTS OF THE PARAMETRIC HAMILTONIAN.  
FITTED VALUES ARE FOR  $\text{Nd}^{3+}:\text{LaCl}_3$ .<sup>a</sup>

		Fitted Value ( $\text{cm}^{-1}$ )	HF Value ( $\text{cm}^{-1}$ )
$H_E$ (Electrostatic Term)	$F^2$	71866	102720
	$F^4$	52132	64462
	$F^6$	35473	46386
$E_E = \sum_{k=0}^6 f_k F^k$ (k-even)			
$H_{SO}$ (Spin-Orbit Interaction)	$\zeta_f$	880	950.5
$E_{SO} = A_{SO} \zeta_f$			
$H_{CF(2)}$ (Two-body Configuration Interaction)	$\alpha$	22.1	28
	$\beta$	-650	-615
	$\gamma$	1586	1611
$E_{CF(2)} = \alpha L(L+1) + \beta G(G_2) + \gamma G(R_7)$			
$H_{CF(3)}$ (Three Particle Configuration Interaction Operators)	$T^2$	377	394
	$T^3$	40	-34
	$T^4$	63	89
$E_{CF(3)} = \sum_i t_i T^i(d)$	$T^6$	-292	-214
	$T^7$	358	314
	$T^8$	354	274
Electrostatically Correlated Spin-Orbit Interaction			
(Two-Body Pseudo Magnetic Operators)	$P^2$	225	
	$P^4$	R	
	$P^6$	R	
Spin-other-orbit and spin-spin effects: Marvin Integrals	$M^0$ $M^2$ $M^4$		HF values used directly
Crystal Field Interaction	$\sum_{k,q,i} B_q^k (C_q^{(k)})_i$		(terms appropriate to the crystal symmetry)

TABLE I-2. Comparison of Values of Free-Ion Parameters (cm<sup>-1</sup>).

	HFR <sup>a</sup>	Pr(IV) <sup>c</sup> Free-Ion	Pr <sup>3+</sup> :LaCl <sub>3</sub> <sup>d</sup>
F <sup>2</sup>	98723	72553	68368
F <sup>4</sup>	61937	53681	50008
F <sup>6</sup>	44564	36072	32743
$\zeta$	820.22	769.91	744
$\alpha$	(28) <sup>b</sup>	23.786	22.9
$\beta$	(-615) <sup>b</sup>	-613.24	-674
$\gamma$	(1611) <sup>b</sup>	745.73	1520
M <sup>0</sup>	1.991	1.588	1.76
P <sup>2</sup>	-	-	275

<sup>a</sup>Reference 20.<sup>b</sup>Reference 11.<sup>c</sup>Reference 21.<sup>d</sup>Reference 12.

TABLE I-3. Crystal Field Parameter Fits for  $\text{Nd}^{3+}:\text{LaCl}_3$  (in  $\text{cm}^{-1}$ ).

	A <sup>a</sup>	B <sup>b</sup>	C <sup>c</sup>
F <sup>2</sup>	73686	72959(76) <sup>d</sup>	71866(42)
F <sup>4</sup>	52996	52318(317)	52132(77)
F <sup>6</sup>	39429	34384(156)	35473(41)
$\alpha$		21.4(0.6)	22.08(0.1)
$\beta$		-650(33)	-650(5)
$\gamma$		1770(59)	1586(12)
T <sup>2</sup>			377(15)
T <sup>3</sup>			40(1)
T <sup>4</sup>			63(3)
T <sup>6</sup>			-292(5)
T <sup>7</sup>			358(8)
T <sup>8</sup>			354(11)
$\zeta$	884.58	878(4)	880(1)
M <sup>k</sup>			(HF)
P <sup>2</sup>			255(23)
B <sub>0</sub> <sup>2</sup>	195	68(65)	163(8)
B <sub>0</sub> <sup>4</sup>	-309	-309(178)	-336(22)
B <sub>0</sub> <sup>6</sup>	-711	-730(174)	-713(22)
B <sub>6</sub> <sup>6</sup>	466	463(138)	462(17)
$\sigma$	>100	>65	8.1
No. of Levels	22	101	101

<sup>a</sup>J. C. Eisenstein, J. Chem. Phys. 39, 2134 (1963).

<sup>b</sup>Fit same data as (c).

<sup>c</sup>Reference 19.

<sup>d</sup>Numbers in parentheses are the rms errors on the parameter values.

TABLE I-4. Comparison of Crystal Field Parameters for the  $4f^4$  and  $5f^4$  ions  $Pm^{3+}$  and  $Np^{3+}$ , diluted in  $LaCl_3$ , with those computed for  $Np^{3+}$  based on point charge considerations.<sup>a</sup>

	$Np^{3+}$	$Pm^{3+}$	$Pr^{3+}$	Predicted $B_q^k (Np^{3+})^b$
				Scaled on $Pm^{3+}$
				Scaled on $Pr^{3+}$
$B_0^2$ ( $cm^{-1}$ )	165(26)	143(18)	107	290
$B_0^4$ ( $cm^{-1}$ )	-623(44)	-395(29)	-342	-1317
$B_0^6$ ( $cm^{-1}$ )	-1615(48)	-666(30)	-677	-3229
$B_6^6$ ( $cm^{-1}$ )	1041(33)	448(21)	466	2172
$\langle r^2 \rangle$ (a.u.)	2.36	1.16	1.356	1.505
$\langle r^4 \rangle$ (a.u.)	11.65	3.49	4.673	
$\langle r^6 \rangle$ (a.u.)	107.6	22.19	33.32	

<sup>a</sup>Reference 7.

<sup>b</sup>Derived from the expression  $(\langle r^n \rangle_{Np^{3+}} / \langle r^n \rangle_{Ln^{3+}}) B_q^k (Ln^{3+})$ , where  $Ln = Pm$  or  $Pr$ .

TABLE I-5. Comparison of Crystal Field Parameters.

$\text{Nd}^{3+}:\text{LaF}_3$		$\text{Nd}^{3+}:\text{LaCl}_3$ <sup>c</sup>
$B_0^2$	$276^a \text{ cm}^{-1}$	$210^b \text{ cm}^{-1}$
$B_0^4$	1408	1239
$B_0^6$	1600	1500
$B_6^6$	679	773
		$\sigma = 16 \text{ cm}^{-1}$
		145 levels fitted
		$\sigma = 8.1 \text{ cm}^{-1}$
		101 levels fitted
$\text{Er}^{3+}:\text{LaF}_3$		$\text{Er}^{3+}:\text{LaCl}_3$ <sup>c</sup>
$B_0^2$	$282^a \text{ cm}^{-1}$	$229^b \text{ cm}^{-1}$
$B_0^4$	1160	965
$B_0^6$	773	909
$B_6^6$	463	484
		$\sigma = 12.1 \text{ cm}^{-1}$
		117 levels fitted
		$\sigma = 5.0 \text{ cm}^{-1}$
		80 levels fitted

<sup>a</sup>Reference 34.<sup>b</sup>Reference 36.<sup>c</sup>Reference 19,21.

TABLE I-6. Crystal-field Parameter Values (in terms of  $A_{nm}$  in  $\text{cm}^{-1}$ ) obtained from lattice sum calculations ( $\text{LaF}_3$ ). Only the values of the even ( $nm$ ) components which determine the level energy are given [37].

		$B_q^{(k)}(D_{3h})$		$B_q^{(k)}(C_2)^b$		$B_q^{(k)}(C_2)^c$		$Nd^{3+}:\text{LaF}_3$	
kq	Real <sup>a</sup>	Real	Imag.	Real	Imag.	Real	Imag.	Real	Imag.
20	465	66	0	-145	0	-216	0		
22		-46	79		5	0		-36	0
40	1849	994	0	652	0	700	0		
42		-103	178	422	118	197	71		
44		-56	-96	397	241	229	181		
60	949	844	0	523	0	490	0		
62		17	-30	-793	66	-928	-23		
64		14	24	-113	-342	-131	-449		
66	862	784	0	-442	-442	-427	-653		

<sup>a</sup>Crystal structure data of K. Schylter, *Arkiv Kemi* 5, 73 (1953) similar to results of Onopko [34]. The c-axis is parallel to the  $D_{3h}$  axis.

<sup>b</sup>Crystal structure of Cheetham *et al.* [31], but with the z-axis of the  $A_{nm}$  parallel to the crystal axis.

<sup>c</sup>Crystal structure of Cheetham *et al.* [31] with the z-axis of the  $A_{nm}$  perpendicular to the crystal axis.

<sup>d</sup>Limited fit of experimental data for  $Nd^{3+}:\text{LaF}_3$  [37].

TABLE I-7. Crystal Field Parameters ( $\text{cm}^{-1}$ ) for  $\text{Er}^{3+}:\text{LaF}_3$ .

	$D_{3h}$ <sup>a</sup>	$D_{3h}$ -axis <sup>a</sup> $C_{2v}$ -symmetry	$C_2$ -axis <sup>b</sup> $C_2$ -symmetry (real part only)	$C_2$ -axis <sup>a</sup> $C_{2v}$ -symmetry
$B_0^2$	226(18)	220(17)	-228	-226(1)
$B_0^4$	965(39)	953(36)	545	552(3)
$B_0^6$	899(34)	897(41)	275	261(10)
$B_6^6$	477(26)	478(30)	-307	-460(22)
$B_2^2$		69(22)	-119	-87(12)
$B_2^4$		67(57)	301	276(9)
$B_4^4$		-40(70)	358	415(10)
$B_2^6$		-36(67)	-520	-620(11)
$B_4^6$		144(54)	56	1(23)
$\sigma$	16	14	17	16

<sup>a</sup>Present work, 117 of 183 states assigned.

<sup>b</sup>Reference 37.

TABLE II-1. Energy Level Parameters for  $\text{Ln}^{3+}$  (aquo).

	$\Omega_2 \times 10^{20}$ $\text{cm}^2$	$\Omega_4 \times 10^{20}$ $\text{cm}^2$	$\Omega_6 \times 10^{20}$ $\text{cm}^2$
$\text{Pr}^{3+}$	28.0 $\pm$ .72	5.89 $\pm$ 2.50	32.2 $\pm$ 3.0
$\text{Nd}^{3+}$	2.25 $\pm$ 1.7	4.08 $\pm$ .80	9.47 $\pm$ 1.3
$\text{Pm}^{3+}$	1.30 $\pm$ .26	4.36 $\pm$ .48	3.94 $\pm$ .34
$\text{Sm}^{3+}$	1.08 $\pm$ .42	3.67 $\pm$ .70	2.87 $\pm$ .56
$\text{Eu}^{3+}$ <sup>a</sup>	(1.46)	(6.66)	(5.40)
$\text{Gd}^{3+}$	1.94 $\pm$ .43	5.27 $\pm$ 1.7	4.46 $\pm$ 1.1
$\text{Tb}^{3+}$	2.76 $\pm$ 5.3	7.95 $\pm$ 6.2	2.87 $\pm$ 1.0
$\text{Dy}^{3+}$	.584 $\pm$ 6.3	3.54 $\pm$ .74	3.90 $\pm$ .62
$\text{Ho}^{3+}$	.791 $\pm$ .79	3.13 $\pm$ .40	2.86 $\pm$ .26
$\text{Er}^{3+}$	1.34 $\pm$ .37	2.19 $\pm$ .25	1.88 $\pm$ .11
$\text{Tm}^{3+}$	.646 $\pm$ 1.0	2.31 $\pm$ .60	1.47 $\pm$ .20

<sup>a</sup>For comparison with other members of the series, the parameters for  $\text{Eu}^{3+}$  were adjusted for the effects of a low-lying excited state [9].

TABLE II-2. Radial Integrals for Selected Trivalent Lanthanides. Radial Integrals (atomic units).<sup>a</sup>

Integral	$\text{Nd}^{3+}(\text{f}^3)$	$\text{Er}^{3+}(\text{f}^{11})$	Relativistic Hartree-Fock Calculation					
	(Judd) <sup>b</sup>	(Judd) <sup>b</sup>	$\text{Pr}^{3+}(\text{f}^2)$	$\text{Nd}^{3+}(\text{f}^3)$	$\text{Pm}^{3+}(\text{f}^4)$	$\text{Ho}^{3+}(\text{f}^{10})$	$\text{Er}^{3+}(\text{f}^{11})$	$\text{Tm}^{3+}(\text{f}^{12})$
$4\text{f} \text{r} 5\text{d}$	.869	.615	.778	.735	.699	.562	.547	.534
$4\text{f} \text{r}^3 5\text{d}$	5.17	2.75	3.85	3.47	3.16	2.08	1.97	1.88
$4\text{f} \text{r}^5 5\text{d}$	47.1	19.9	27.8	24.0	20.9	11.7	10.9	10.2
$4\text{f} \text{r}^2 4\text{f}$	1.394	.831	1.19	1.10	1.01	.726	.693	.664
$4\text{f} \text{r}^4 4\text{f}$	4.96	1.95	3.27	2.80	2.44	1.30	1.20	1.11
$4\text{f} \text{r}^6 4\text{f}$	36.4	10.5	17.6	14.1	11.6	4.85	4.36	3.94

 $\alpha_1 \text{ a.u.} = .5292 \times 10^{-8} \text{ cm.}$ 
<sup>b</sup>Reference 44.

TABLE II-3. Energy Differences  $\Delta(f^N + f^{N-1})$  for  $\text{Ln}^{3+}$  corrected for  $\text{Ln}^{3+}(\text{aquo})$  Stabilization Energy.

	Judd <sup>a</sup> (cm <sup>-1</sup> )	This Work <sup>b</sup> (cm <sup>-1</sup> )
$\text{Pr}^{3+}$		45000
$\text{Nd}^{3+}$	58000	56000
$\text{Pm}^{3+}$		59000
$\text{Gd}^{3+}$		78000
$\text{Tb}^{3+}$		38000
$\text{Ho}^{3+}$		63000
$\text{Er}^{3+}$	92000	65000
$\text{Tm}^{3+}$		64000

<sup>a</sup>Reference 44.

<sup>b</sup>From Figs. 1,2 corrected in part using Reference 59.

TABLE II-4. Comparison of Calculated Values of  $\Omega_4$  and  $\Omega_6$  with Those Fit to the Experimental Results for  $\text{Ln}^{3+}(\text{aquo})$ .

	$\Omega_\lambda \times 10^{20} \text{ cm}^2$			
	Fit		Calc'd	
	$\Omega_4$	$\Omega_4$	$\Omega_6$	$\Omega_6$
$\text{Pr}^{3+}$	5.89	1.13	32.2	1.73
$\text{Nd}^{3+}$	4.08	.553	9.47	.791
$\text{Pm}^{3+}$	4.36	.405	3.94	.523
$\text{Gd}^{3+}$	5.27	.127	4.46	.146
$\text{Tb}^{3+}$	7.95	.462	2.87	.515
$\text{Ho}^{3+}$	3.13	.131	2.86	.141
$\text{Er}^{3+}$	2.19	.110	1.88	.116
$\text{Tm}^{3+}$	2.31	.104	1.47	.106

TABLE III-5. Intensity Parameters for the Heavy  $\text{An}^{3+}$  (aquo) Ions.

	$\Omega_2 \times 10^{20} \text{ cm}^2$	$\Omega_4 \times 10^{20} \text{ cm}^2$	$\Omega_6 \times 10^{20} \text{ cm}^2$
$\text{Cm}^{3+}$	15.2	16.8	38.1
$\text{Bk}^{3+}$	6.96	12.2	18.7
$\text{Cf}^{3+}$	3.39	15.4	16.6
$\text{Es}^{3+}$	1.32	15.8	18.5

TABLE III-6. Observed and Calculated Band Intensities for  $\text{Bk}^{3+}$  (aquo).

Band Center ( $\text{cm}^{-1}$ )	$P \times 10^6$		Band Center ( $\text{cm}^{-1}$ )	$P \times 10^6$	
	Expt.	Theory		Expt.	Theory
8000	17.4	14.5	26450	3.46	3.35
9560	7.08	9.24	27100	4.32	3.01
15700	11.7	7.49	28000	0.4	0.2
19840	3.24	2.14	28820	2.76	2.21
21190	32.4	27.7	29675	4.28	1.86
23590	28.5	33.6	30500	8.20	8.68
25250	5.18	4.98			

TABLE II-7. Radial Integrals for Selected Trivalent Actinides. Radial Integrals (atomic units)

Integral	Relativistic Hartree - Fock Calculation					
	$U^{3+}(f^3)$	$Np^{3+}(f^4)$	$Pu^{3+}(f^5)$	$Bk^{3+}(f^8)$	$Cf^{3+}(f^9)$	$Es^{3+}(f^{10})$
$(5f r 5d)$	1.22	1.14	1.07	.911	.869	.831
$(5f r^3 5d)$	7.91	6.95	6.18	4.57	4.20	3.87
$(5f r^5 5d)$	74.4	61.4	51.6	33.3	29.5	26.3
$(5f r^2 5f)$	2.28	2.07	1.90	1.53	1.43	1.35
$(5f r^4 5f)$	10.2	8.42	7.06	4.54	4.00	3.55
$(5f r^6 5f)$	81.8	61.1	47.0	24.4	20.3	17.0

TABLE II-8. Energy Differences  $\Delta(f^N \rightarrow f^{N-1} d)$  for  $An^{3+}$  Corrected for  $An^{3+}(\text{aquo})$  Stabilization Energy.<sup>a</sup>

	$\text{cm}^{-1}$		$\text{cm}^{-1}$
$U^{3+}$	25000	$Cm^{3+}$	(52000)
$Np^{3+}$	32000	$Bk^{3+}$	34000
$Pu^{3+}$	38000	$Cf^{3+}$	46000
$Am^{3+}$	44000	$Es^{3+}$	(57000)

<sup>a</sup>From Figs. II-4, II-6, and II-7.

TABLE II-9. Comparison of Calculated Values of  $\Omega_4$  and  $\Omega_6$  with Those Fit to Experimental Results for  $An^{3+}(\text{aquo})$ .

	$\Omega_\lambda (\times 10^{20} \text{ cm}^2)$			
	Fit	Calc'd	Fit	Calc'd
	$\Omega_4$	$\Omega_4$	$\Omega_6$	$\Omega_6$
$U^{3+}$	55 <sup>a</sup>	33.1	186 <sup>a</sup>	80.8
$Np^{3+}$	77 <sup>a</sup>	14.3	155 <sup>a</sup>	31.3
$Pu^{3+}$	26 <sup>a</sup>	7.41	66 <sup>a</sup>	14.8
$Cm^{3+}$	16.8	2.28	38.1	3.89
$Bk^{3+}$	12.2	4.21	18.7	6.79
$Cf^{3+}$	15.4	1.86	16.6	2.83
$Es^{3+}$	15.8	.994	18.5	1.44

<sup>a</sup>Estimated values.

TABLE III-1. Radiative Lifetimes of Excited States of  $\text{Ln}^{3+}$  (aquo).

Experimental (msec)					
	Excited State	Energy Gap $\Delta E(\text{cm}^{-1})$	$\tau_{\text{H}_2\text{O}}$	$\tau_{\text{D}_2\text{O}}$	Theory (msec)
Gd <sup>3+</sup>	$6\text{P}_{7/2}$	32,200	2.3 <sup>a</sup>		10.9
Tb <sup>3+</sup>	$5\text{D}_4$	14,800	0.39 <sup>b</sup>	3.3 <sup>b</sup>	9.02
Eu <sup>3+</sup>	$5\text{D}_0$	12,300	0.10 <sup>b</sup>	1.9 <sup>b</sup>	9.67
Dy <sup>3+</sup>	$4\text{F}_{9/2}$	7,400	0.0023 <sup>a</sup>	0.038 <sup>a</sup>	1.85
Sm <sup>3+</sup>	$4\text{G}_{5/2}$	7,400	0.0023 <sup>a</sup>	0.053 <sup>a</sup>	6.26
Pm <sup>3+</sup>	$5\text{F}_1$	5,800			0.65
Nd <sup>3+</sup>	$4\text{F}_{3/2}$	5,380	0.00003 <sup>c</sup>	0.00017 <sup>c</sup>	0.42
Er <sup>3+</sup>	$4\text{S}_{3/2}$	3,100			0.66
Ho <sup>3+</sup>	$5\text{S}_2$	3,000			0.37

<sup>a</sup>Reference 77.<sup>b</sup>Reference 75.<sup>c</sup>Reference 79.

### Figure Captions

FIGURE I-1. No caption.

FIGURE I-2. The free-ion Hamiltonian.

FIGURE I-3. Variation of Slater Integral  $F^2$  with lanthanide atomic number.

FIGURE I-4. Variation of the differences between the pseudo relativistic Hartree-Fock values of the Slater integrals  $F^k$  and those determined experimentally as a function of lanthanide atomic number.

FIGURE I-5. Variation of the spin-orbit integral ( $\zeta$ ) with lanthanide atomic number.

FIGURE I-6. Crystal-field parameters and energy level structure for  $Nd^{3+}(4f^3)$  which has a total of 41 free-ion states and 182 crystal-field states ( $D_{3h}$ -symmetry).

FIGURE I-7. Hartree-Fock calculations for the outer orbitals in  $Nd^{3+}$  and  $U^{3+}$ . The 4f and 5f vertical scales are increased relative to those of the cores [29].

FIGURE I-8. Comparison of the experimentally observed and model computed Stark levels for the  $^5I_7$  state in  $Ho^{3+}:LaF_3$ .

FIGURE I-9. Spectrum of the  $^5I_7$  state of  $Ho^{3+}:LaF_3$  at 4 K.

FIGURE II-1,2. Absorption spectra of the light and heavy trivalent lanthanide aquo ions.

FIGURE II-3. Solution absorption spectra of  $Ho^{3+}$  in (A) tetrabutylammonium nitrate-nitroethane, and (B) in 1 M  $HNO_3$  [53].

FIGURE II-4. Variation of the lowest energy state in the lower-lying configurations of  $Ln^{3+}$  and  $An^{3+}$  with atomic number. The reference energy is that of  $f^N$  [59].

FIGURE II-5. Computed energy span of the  $f^N$ -configurations for the light trivalent lanthanides and actinides.

FIGURE II-6,7. Absorption spectra of the light and heavy trivalent actinide aquo ions.

FIGURE II-8. Absorption spectra of the aquo ions of  $Tb^{3+}(4f^8)$  and  $Bk^{3+}(5f^8)$ .

FIGURE III-1. Fluorescing states of  $\text{Ln}^{3+}$  (aquo) as reported in papers published by Deutschbein, Mehnert and Tomaschek, summarized in reference 43.

FIGURE III-2. Computed fluorescence branching ratios for  $\text{Tb}^{3+}$  (aquo) and for  $\text{Tb}(\text{NO}_3)_3$  in a molten  $\text{LiNO}_3$ - $\text{KNO}_3$  eutectic at 150°.

FIGURE III-3. Fluorescence spectrum of the gas phase  $\text{TbCl}_3(\text{AlCl}_3)_x$  complex at 535 K showing the bands arising from the  $5\text{D}_4 \rightarrow 7\text{F}_0 - 7\text{F}_6$  transitions.

FIGURE III-4. Computed radiative branching ratios for the heavier  $\text{An}^{3+}$  aquo ions.

FIGURE III-5.  $\text{Ln}^{3+}$  (aquo) non-radiative decay rate versus energy gap in  $\text{H}_2\text{O}$  and  $\text{D}_2\text{O}$  solutions. —  $\text{H}_2\text{O}$ , - - -  $\text{D}_2\text{O}$ .

Schrödinger's Equation for the Steady State of a Many Electron System

$$H\psi = E\psi$$



Central Field Approximation -- Each Electron Moving in the Central Field  $U(r_i)$  Satisfies

$$\left[ -\frac{\hbar^2}{2m} \nabla^2 + U(r) \right] \phi(a_i) = E(a_i) \phi(a_i)$$



Hartree-Fock Approach

Parametric Approach

FIGURE I-1.

FIGURE 2. The Free-Ion Hamiltonian.

The total energy of a system consisting of a point nucleus surrounded by N electrons can be represented by the Hamiltonian:

$$H = H_0 + H_E + H_{SO}$$

$H_0$  (involves the kinetic energy of the electrons and their interaction with the nucleus)

$$H_E \text{ (electrostatic term)} \quad E_e = \sum_{k=0}^6 f_k F^k \text{ (k even)}$$

$$H_{SO} \text{ (spin-orbit interaction)} \quad E_{SO} = A_{SO} \quad f$$

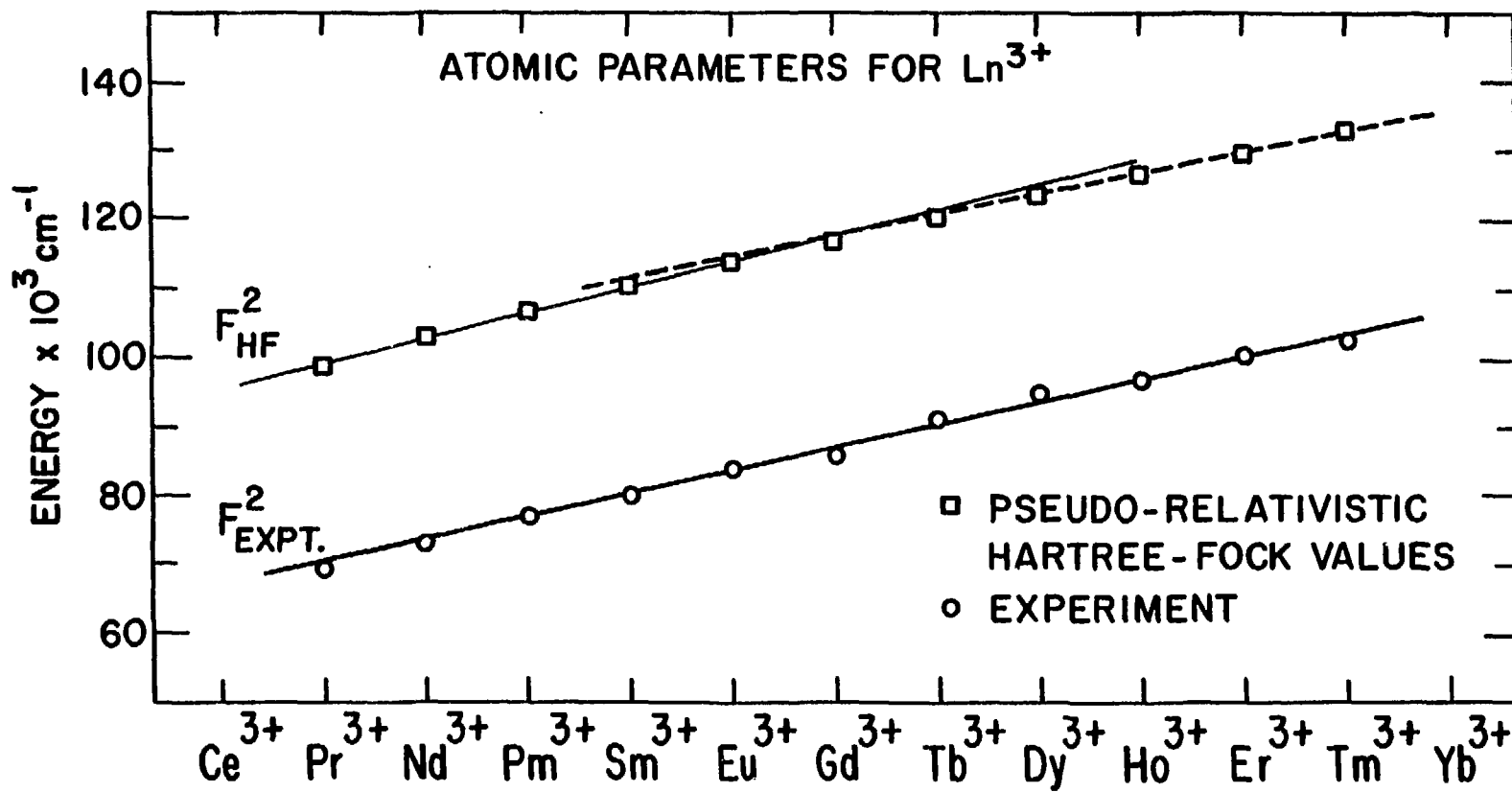


FIGURE I-3.

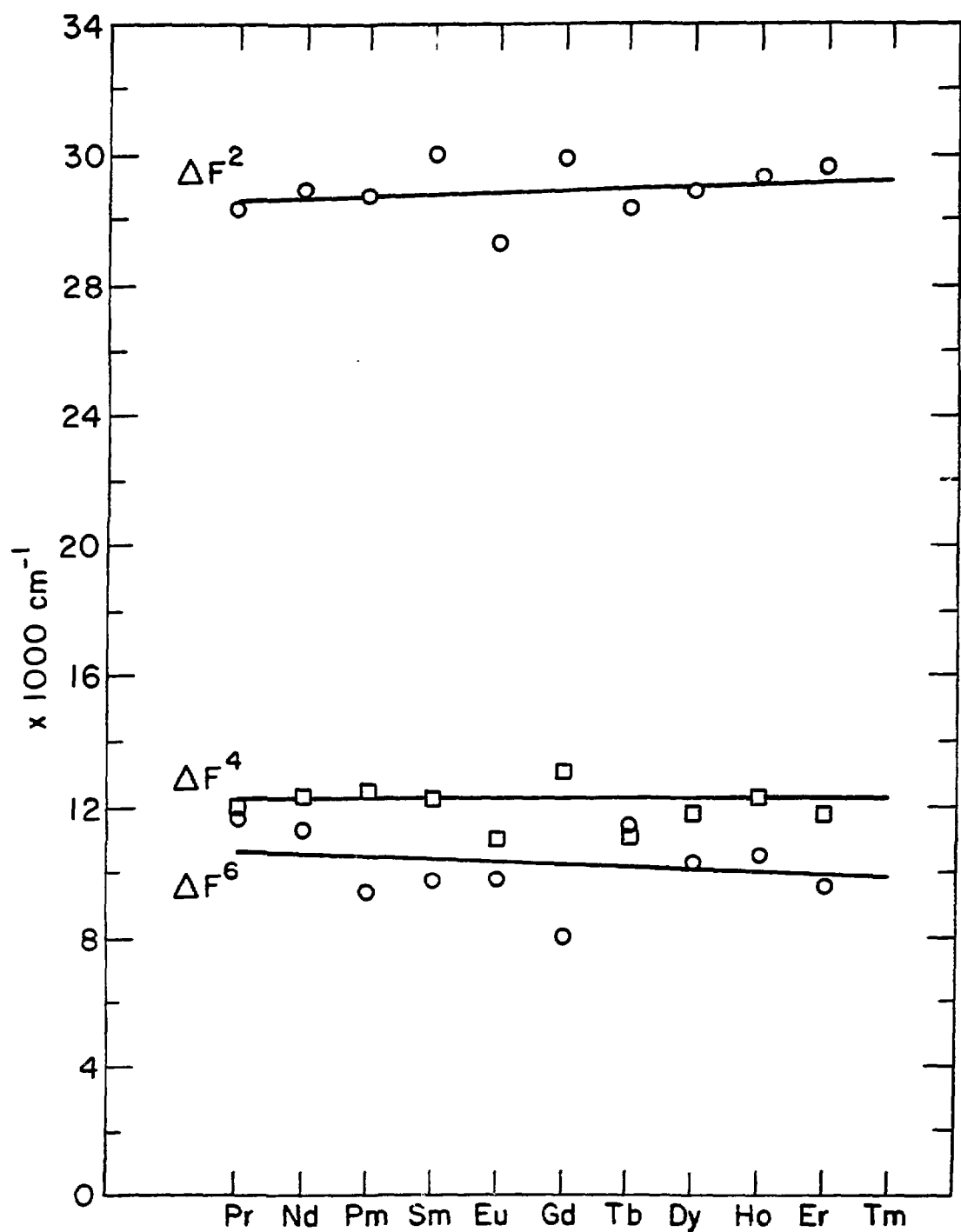


FIGURE I-4.

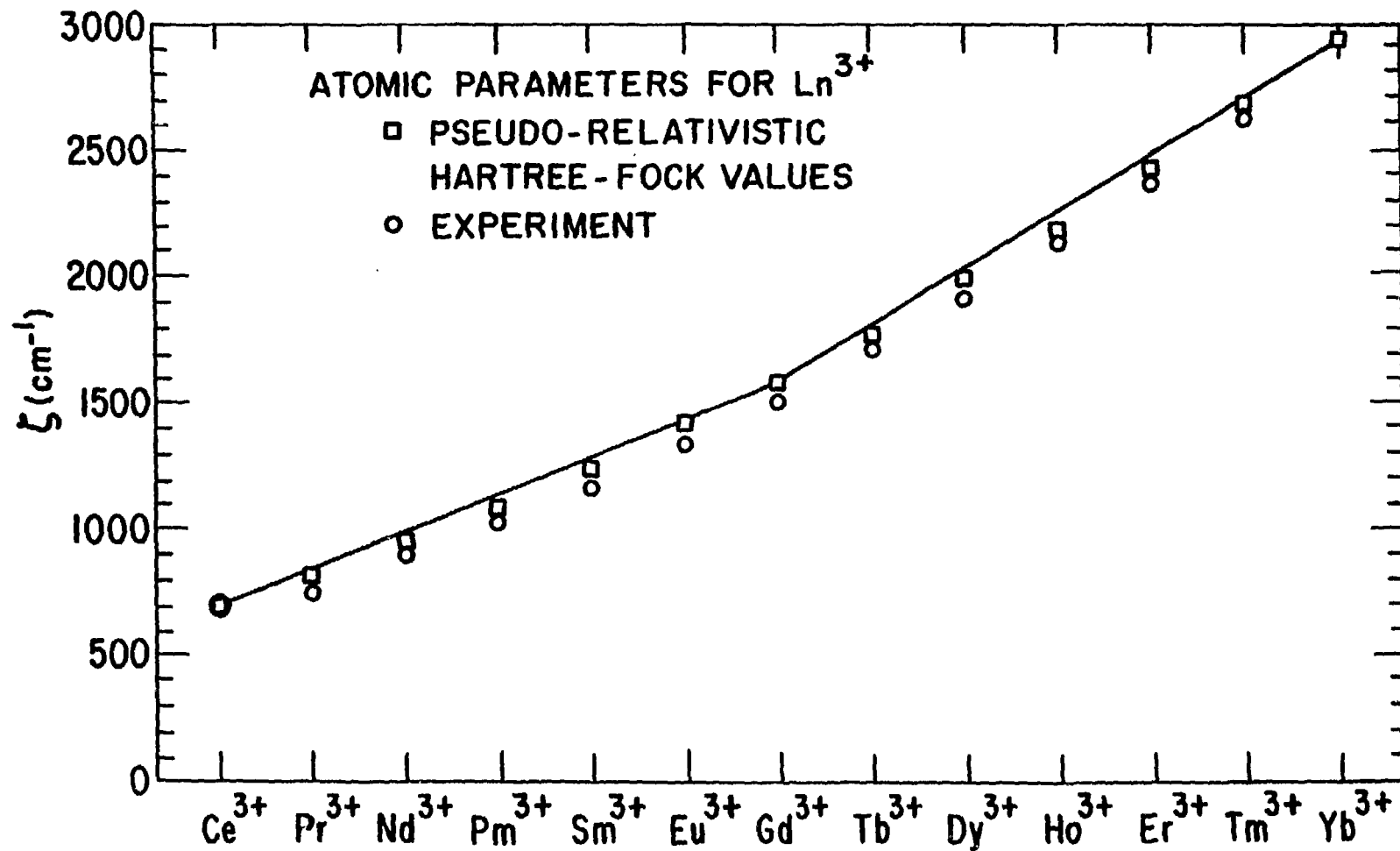
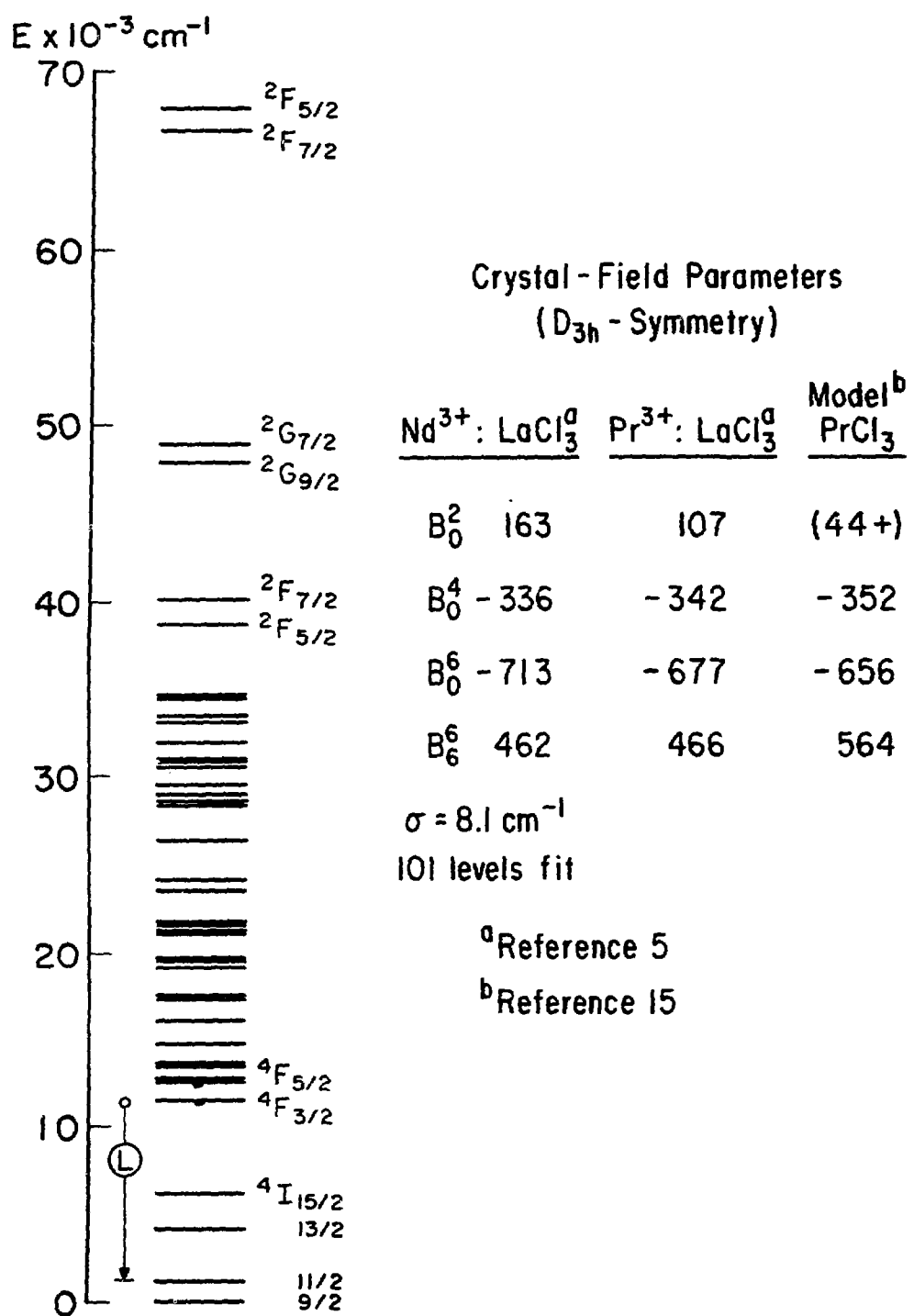


FIGURE I-5.

FIGURE I-6.



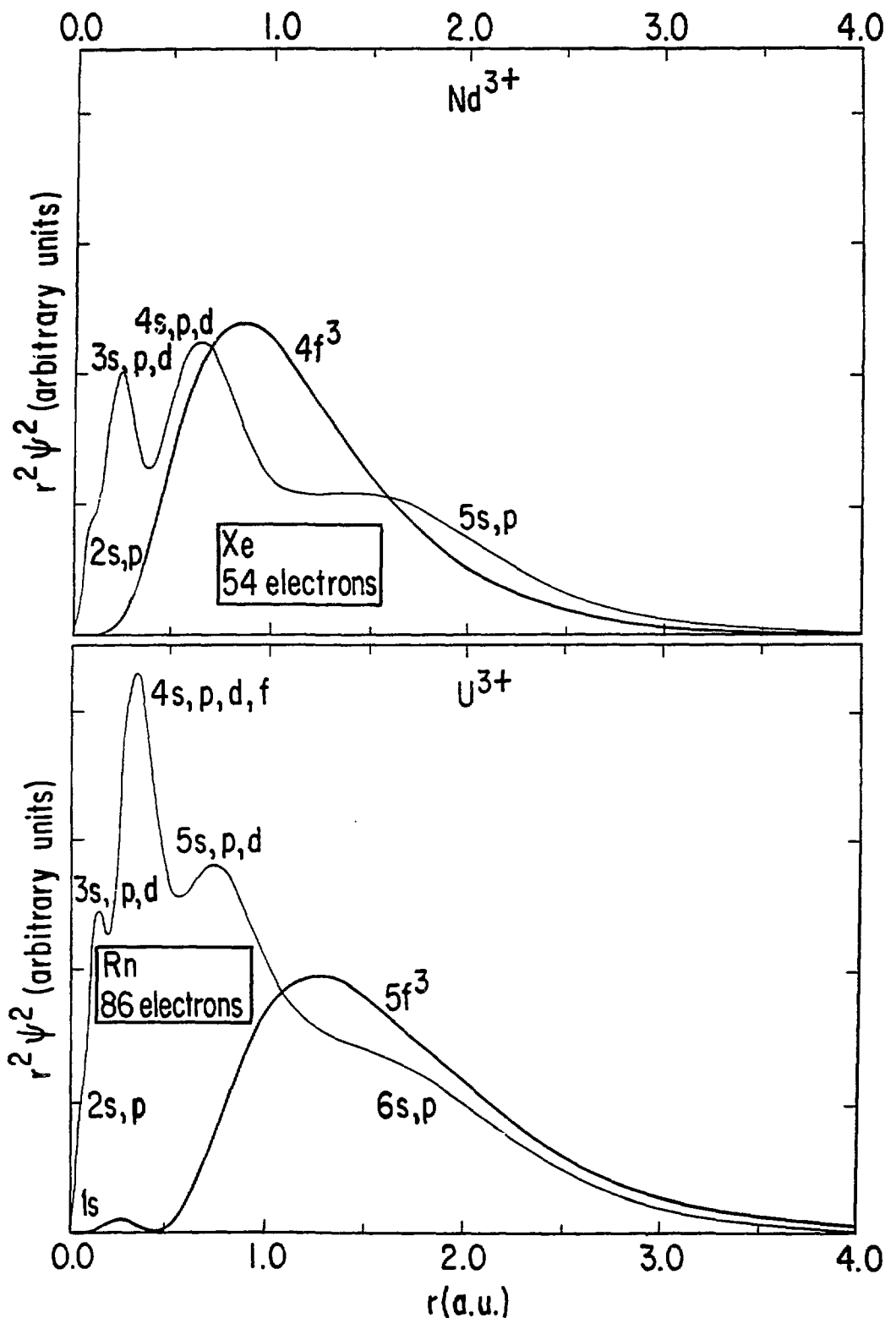


FIGURE I-7.

COMPARISON OF THE EXPERIMENTALLY OBSERVED AND MODEL COMPUTED  
STARK LEVELS FOR THE  $5I_7$  STATE IN  $Ho^{3+}:LaF_3$

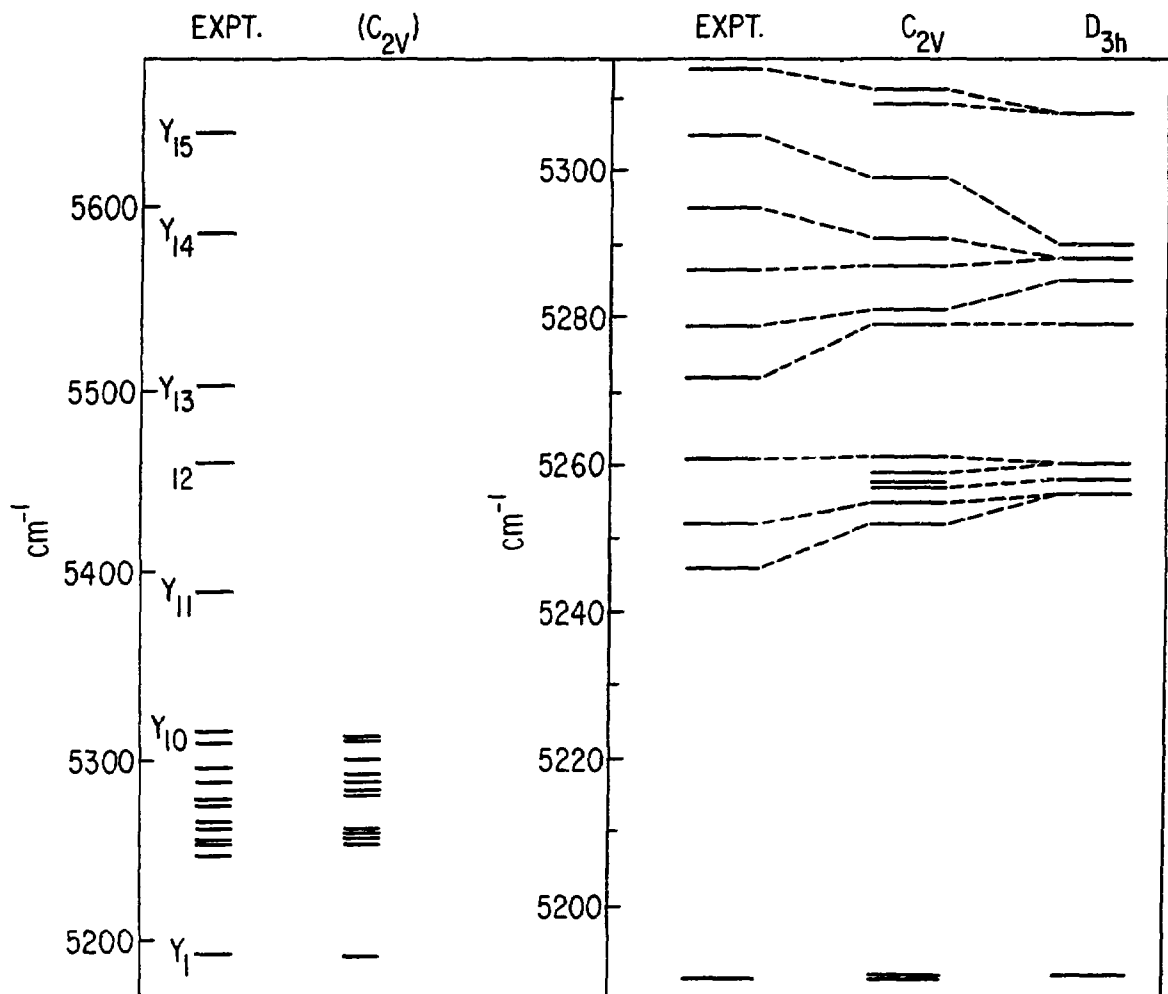


FIGURE I-8.

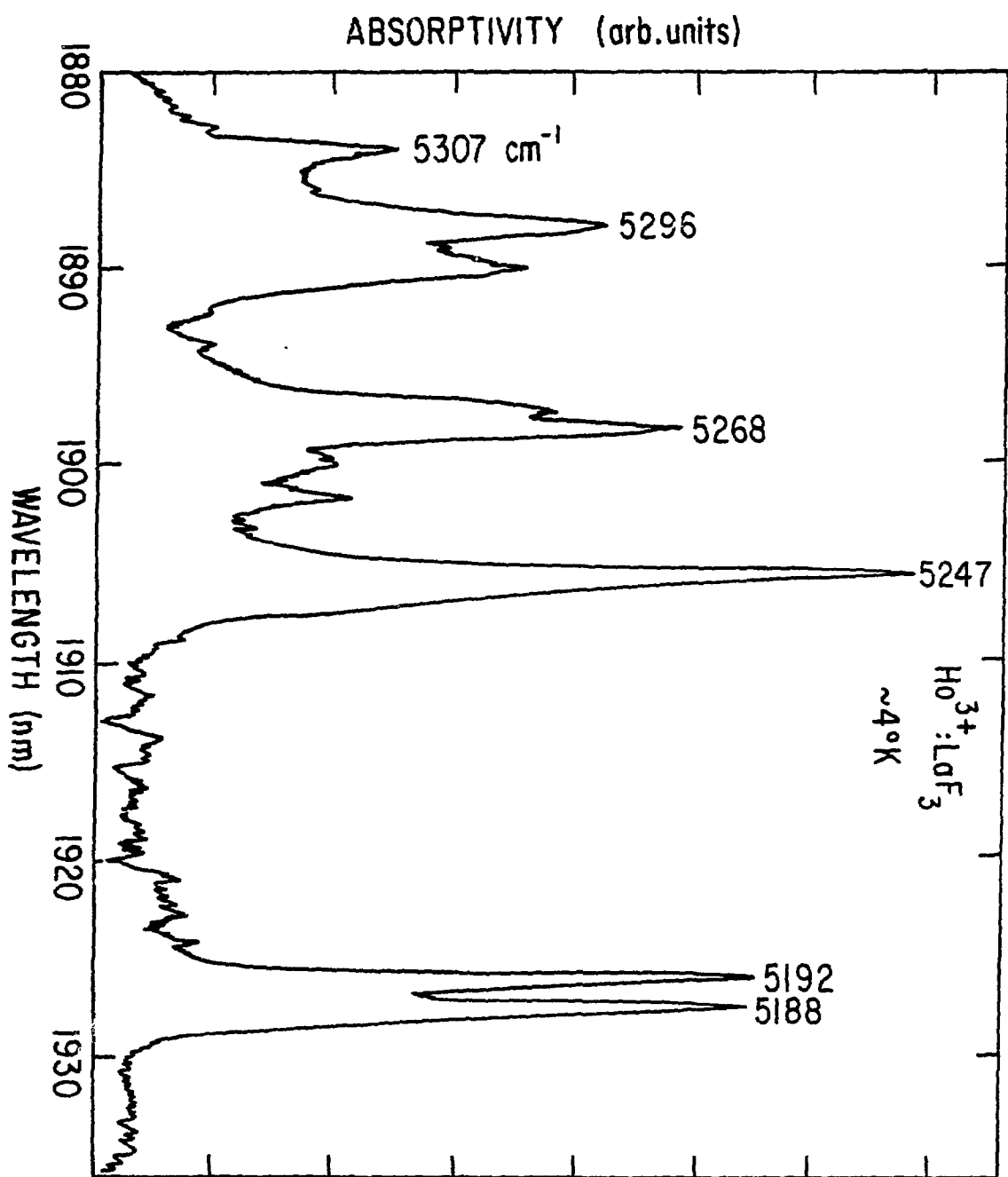


FIGURE I-9.

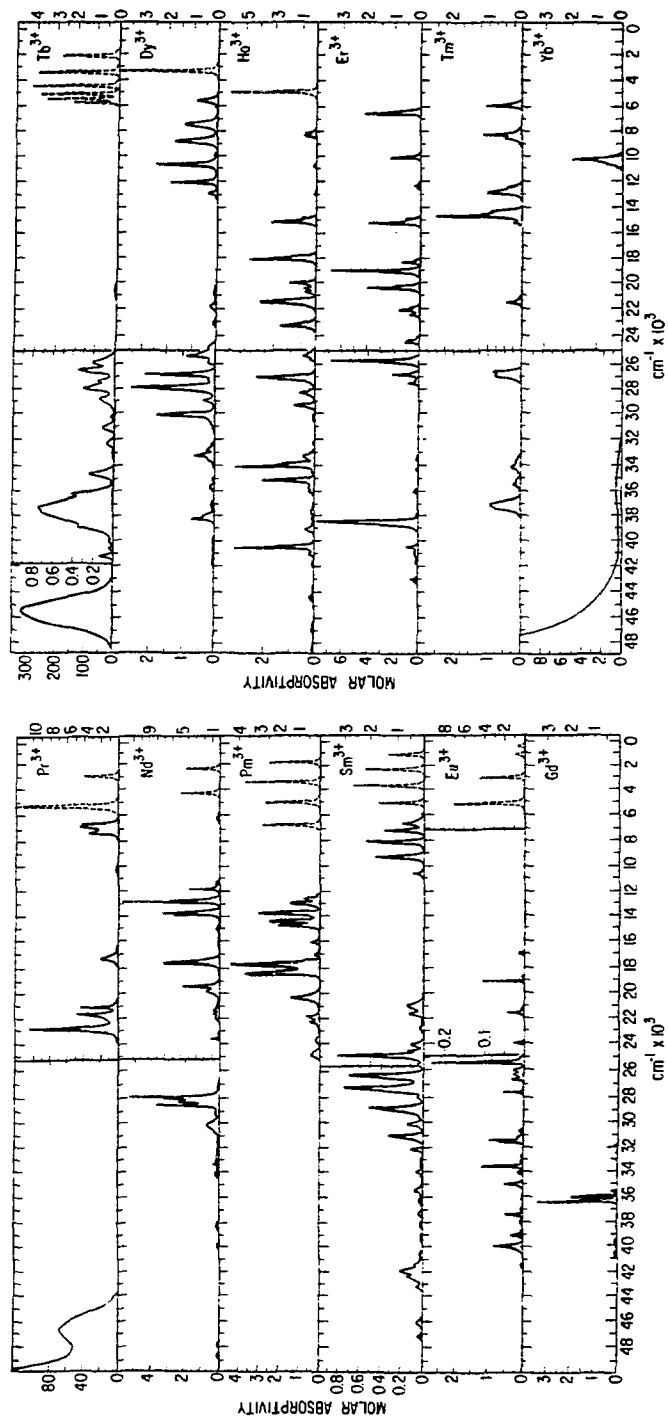


FIGURE III-1,2.

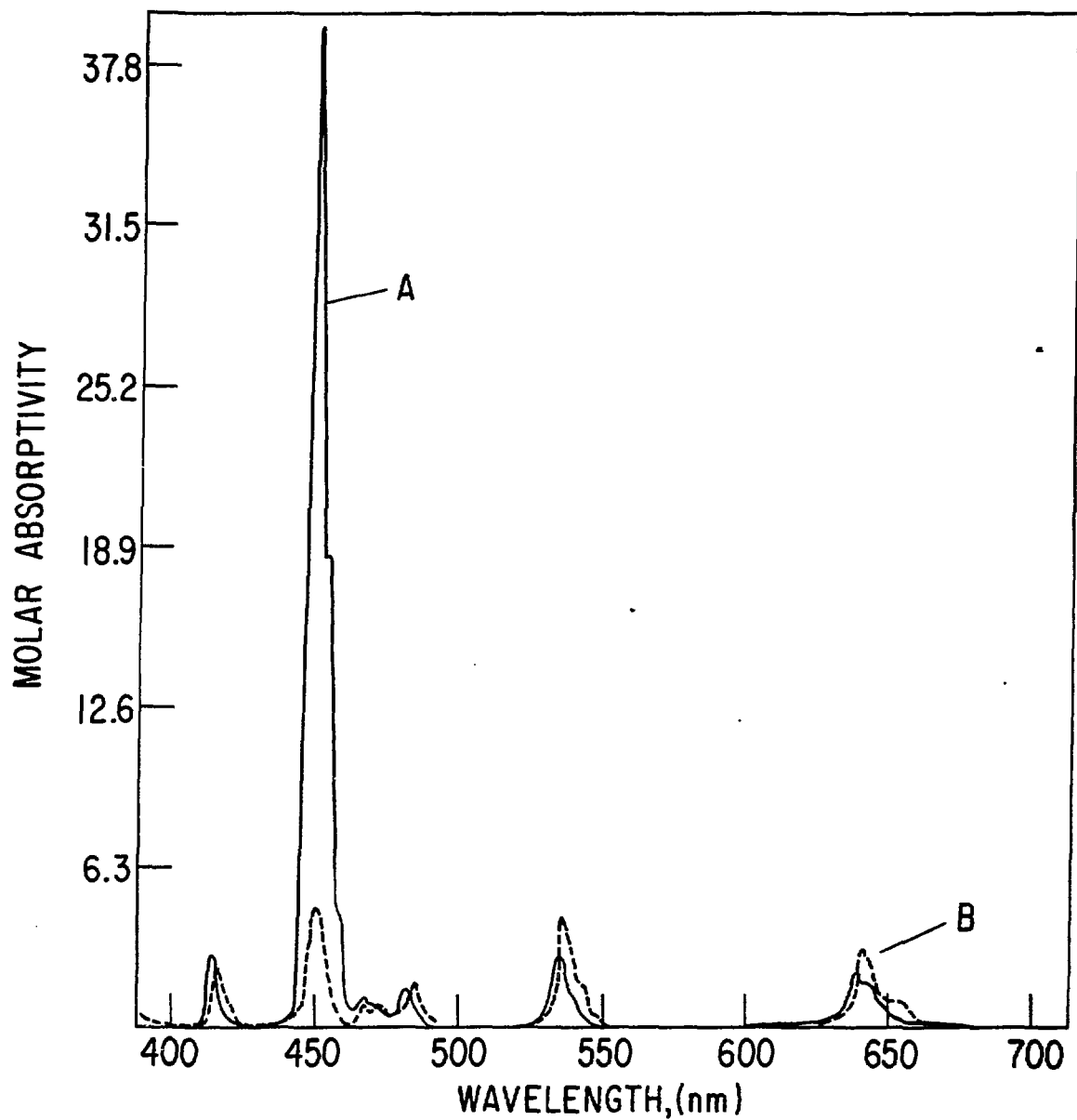


FIGURE II-5.

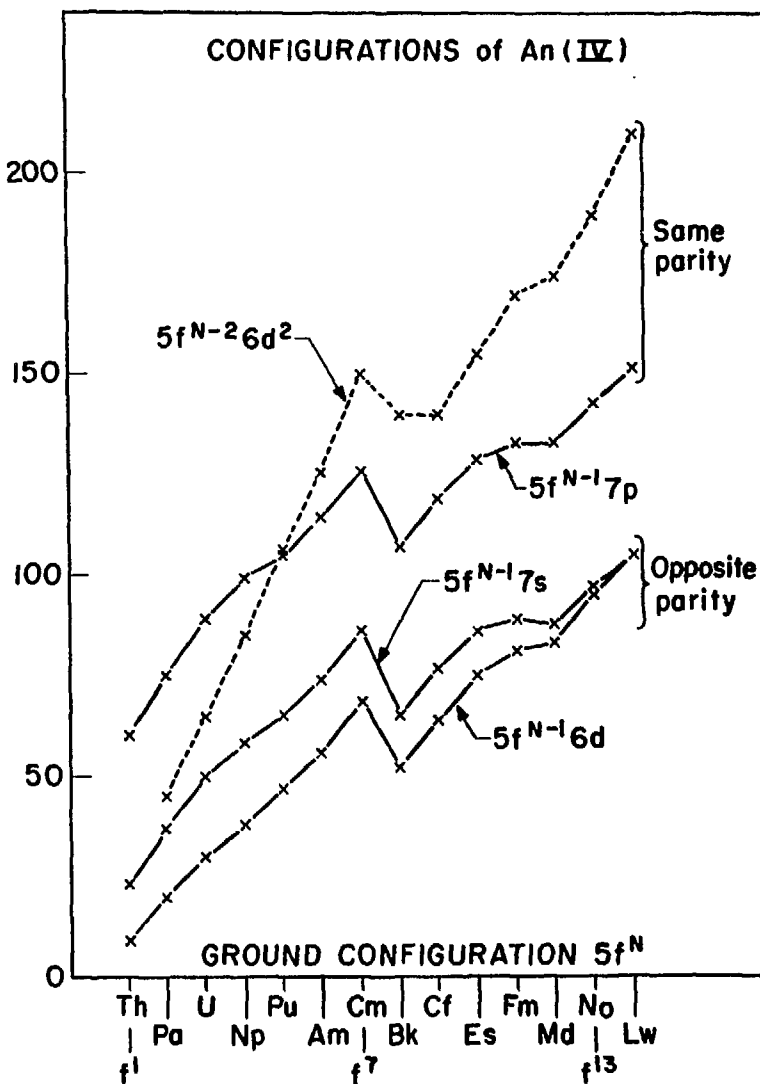
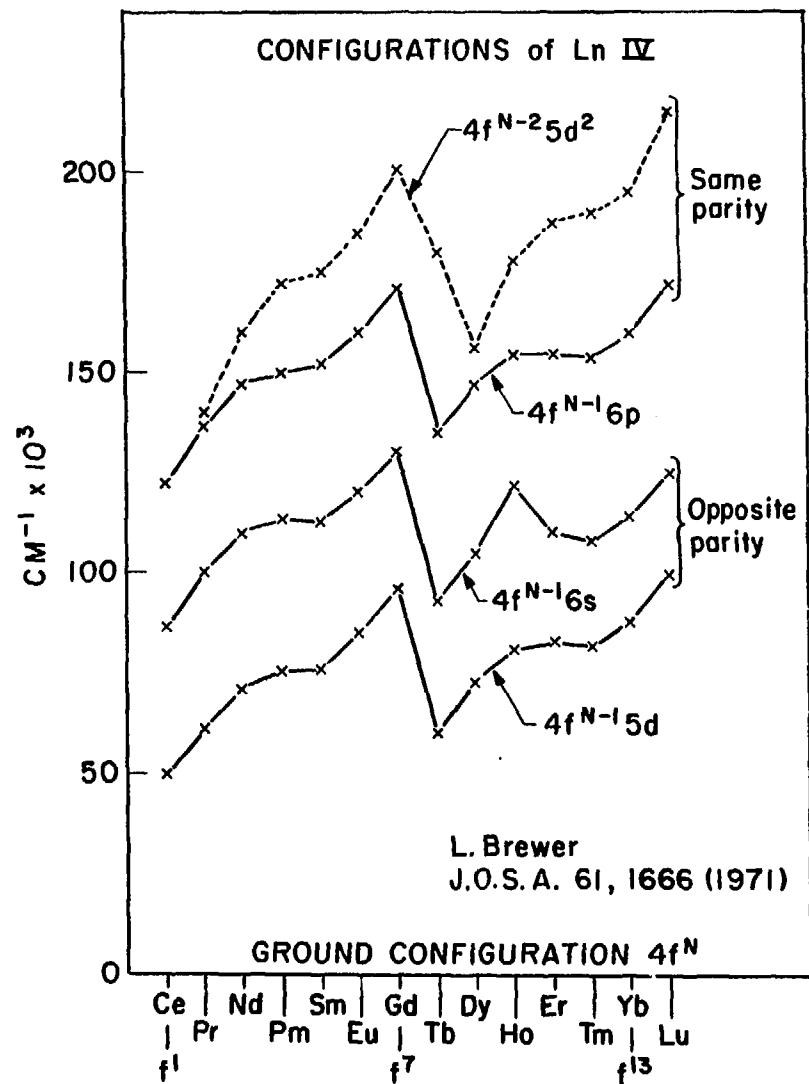


FIGURE II-4.

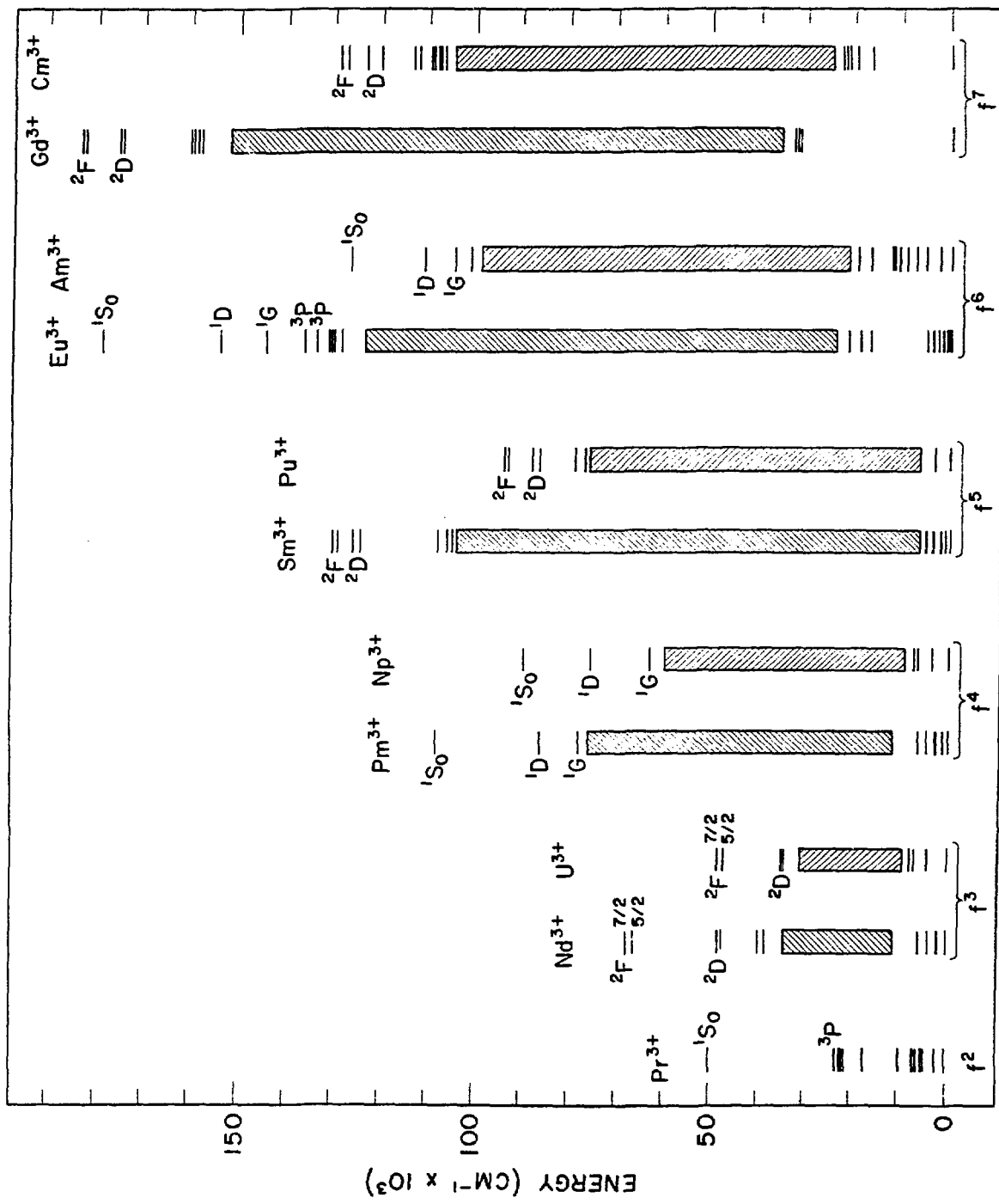


FIGURE 11-5.

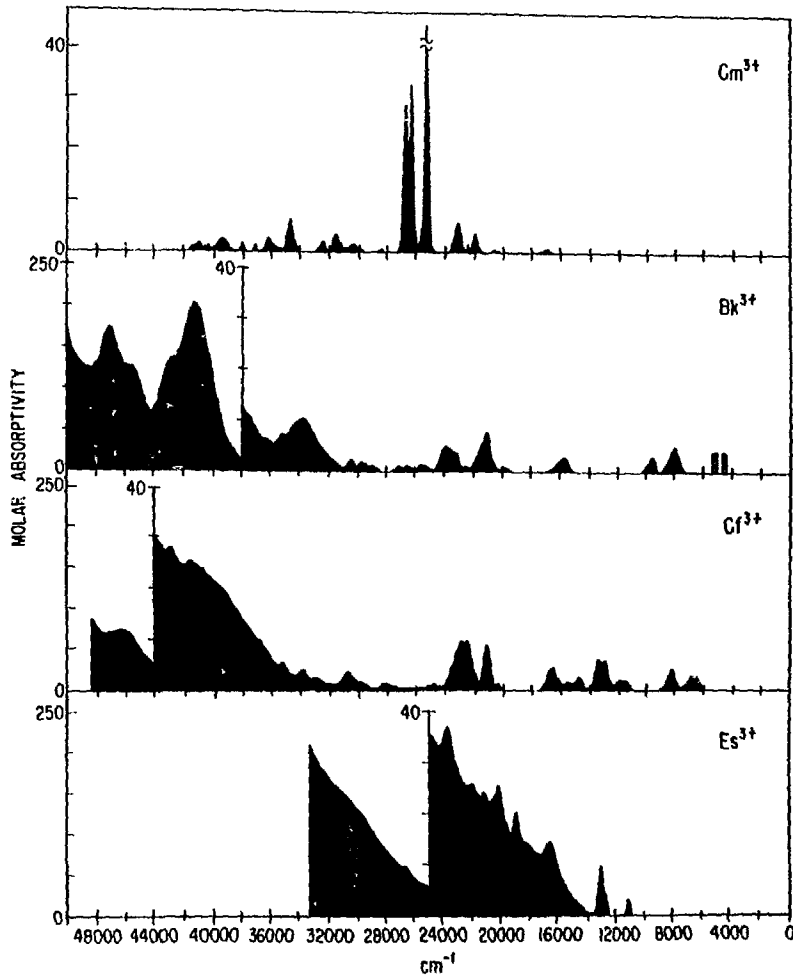
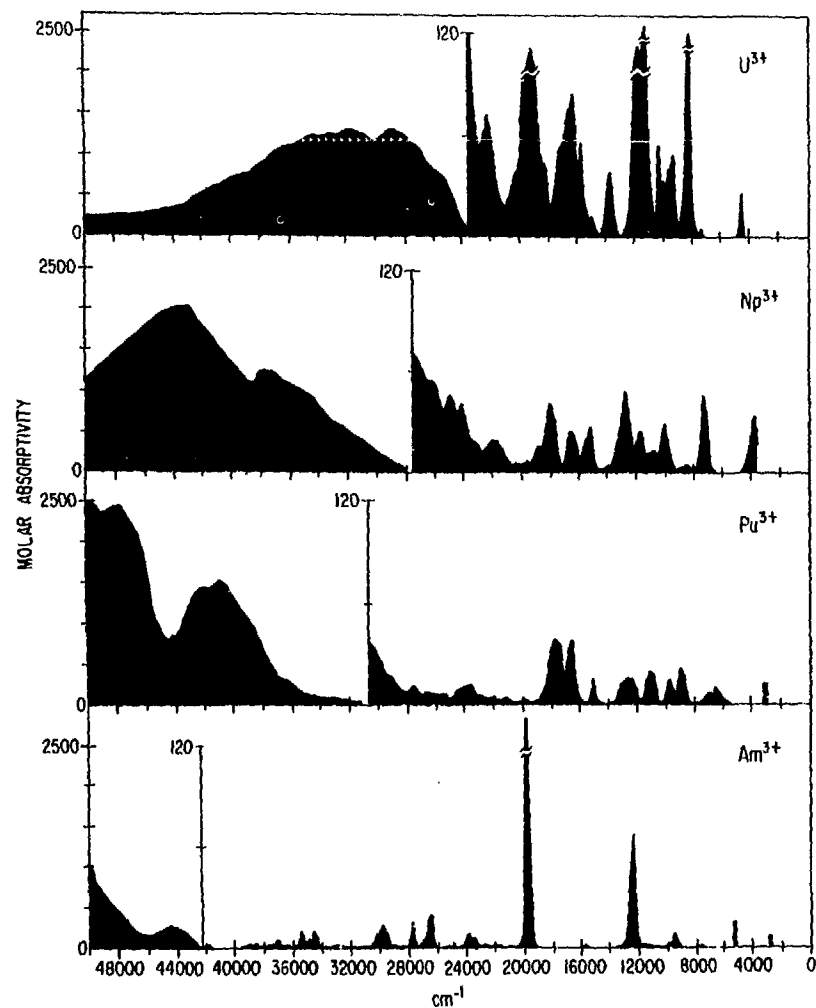


FIGURE II-6,7.

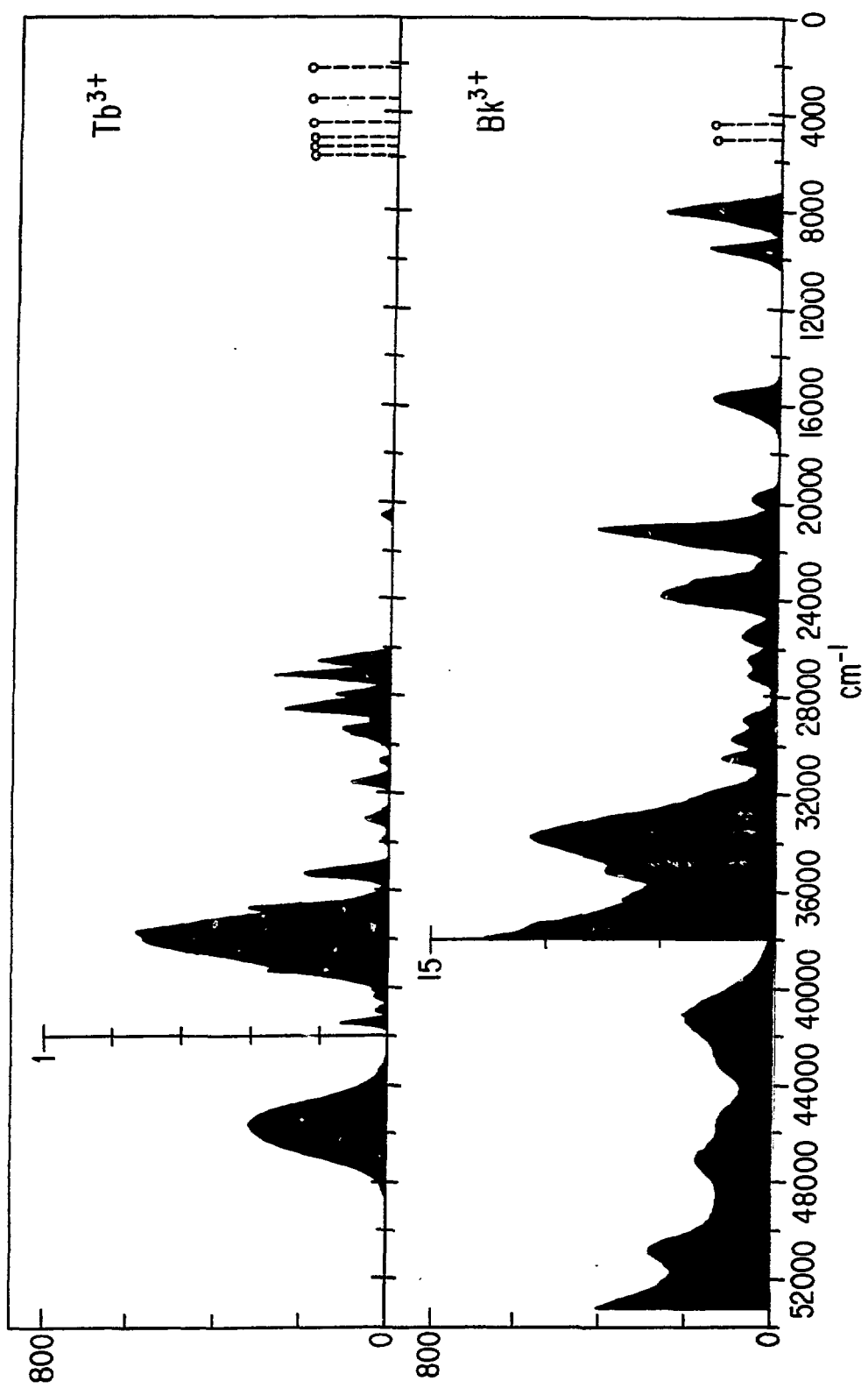


FIGURE 11-8.

### FLUORESCENCE IN AQUEOUS SOLUTION

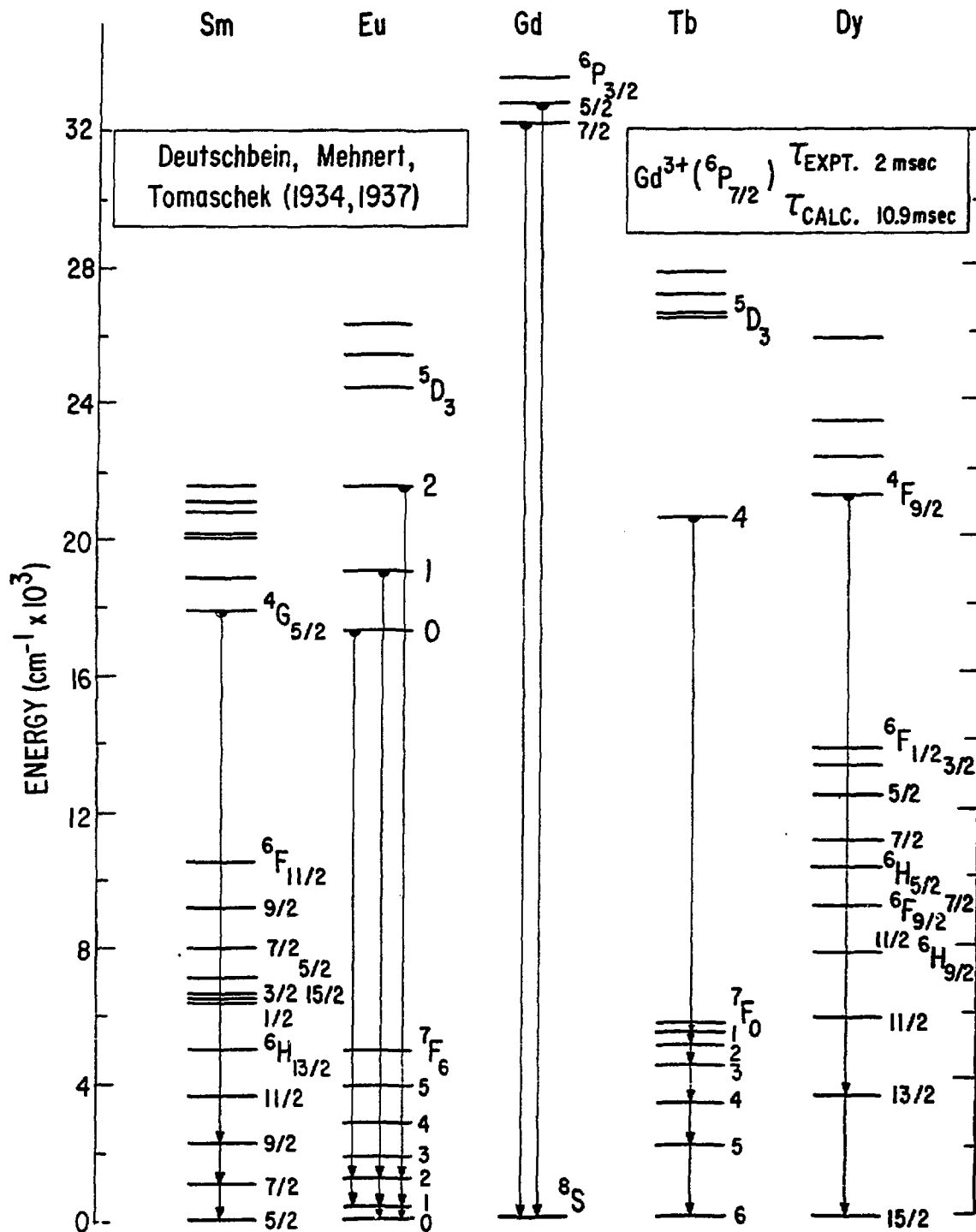


FIGURE III-1.

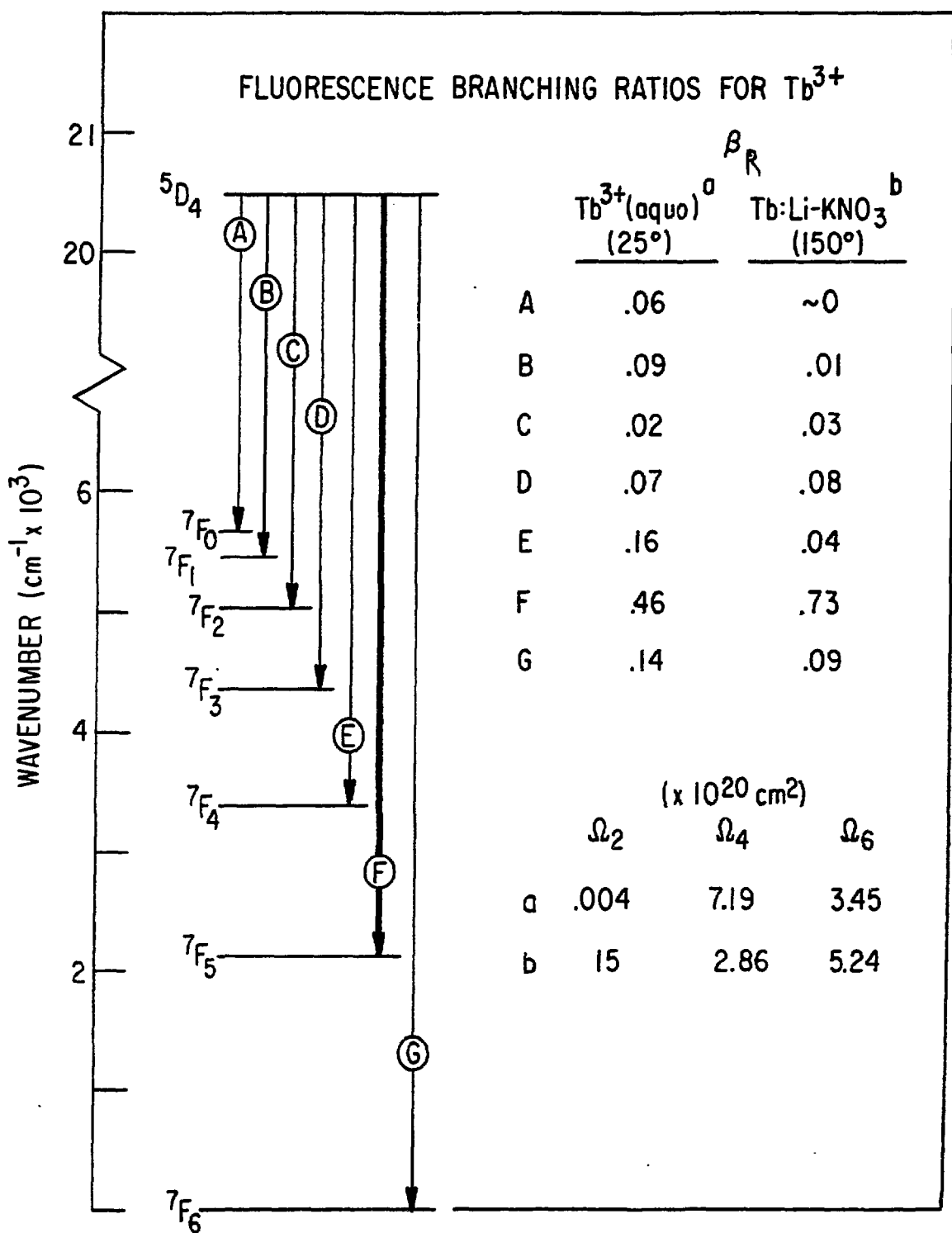


FIGURE III-2.

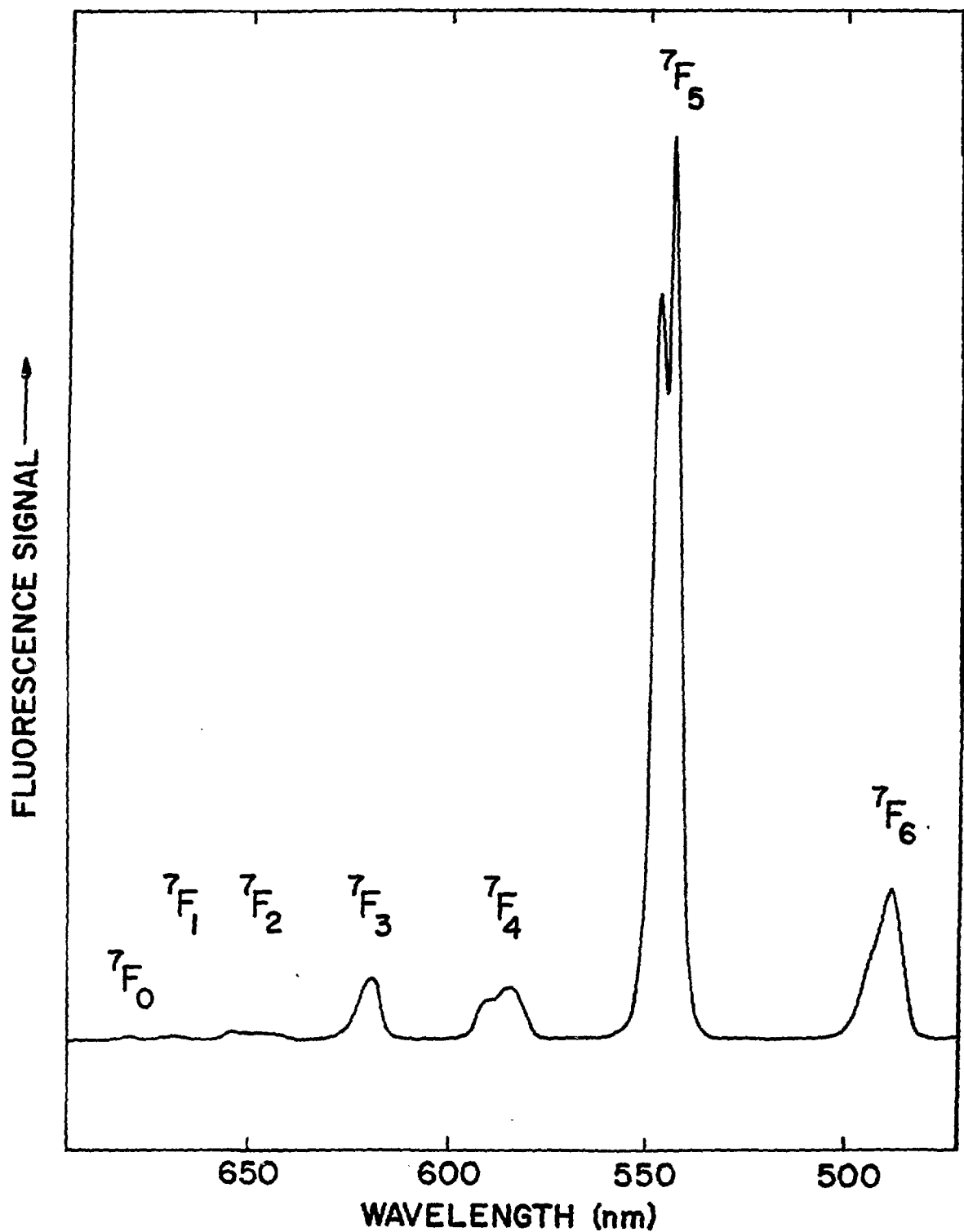


FIGURE III-3.

### SELECTED RADIATIVE BRANCHING RATIOS

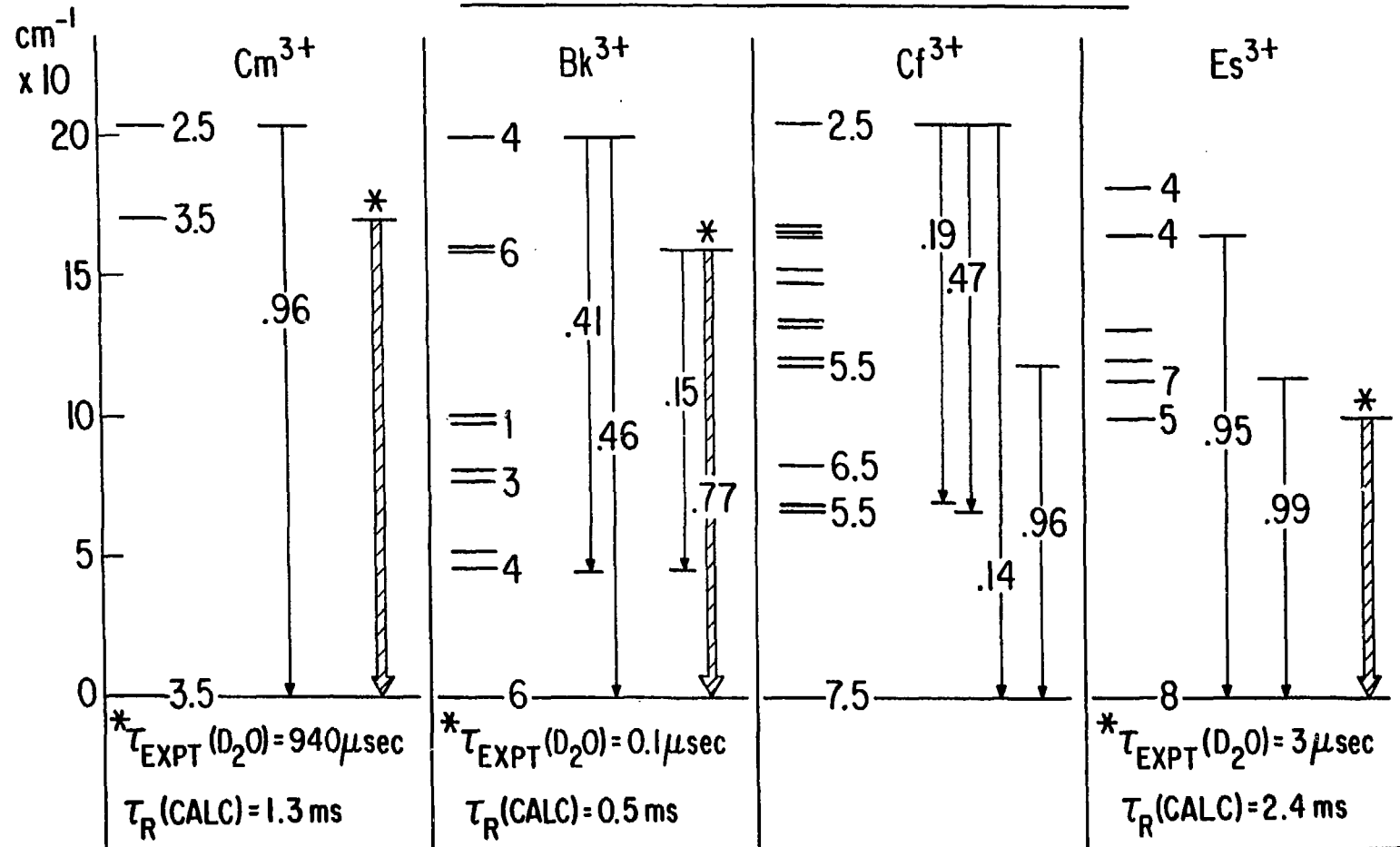
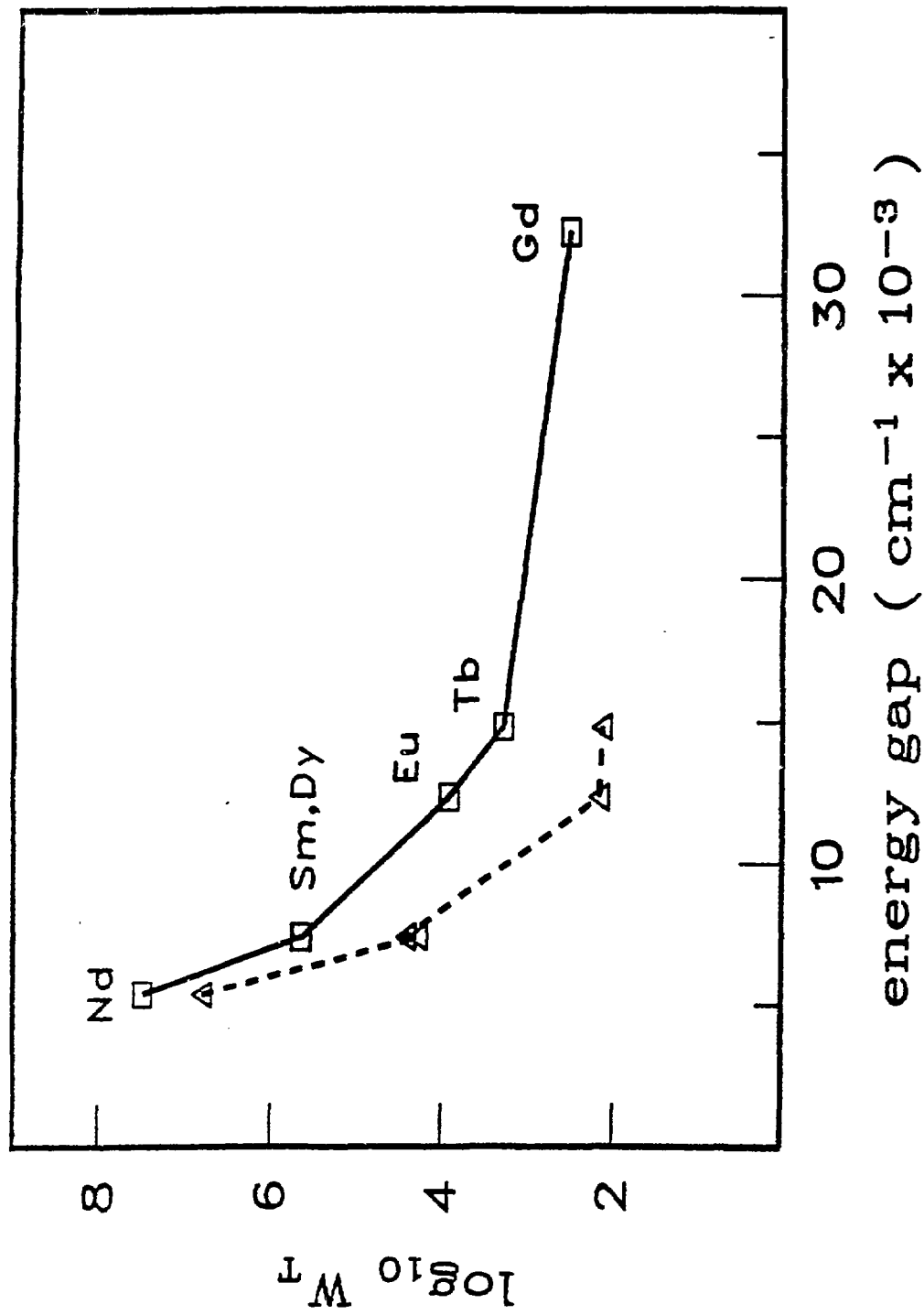


FIGURE III-4.

FIGURE III-5.

$\tau_1/\tau$



A HERD OF SMALL WHITE DEER (A RARE MUTATION OF THE FALLOW DEER, *DAMA DAMA*) ROAM THE ARGONNE GROUNDS.  
THE DRAWING ON THE COVER SHOWS THREE OF THESE UNUSUAL ANIMALS.